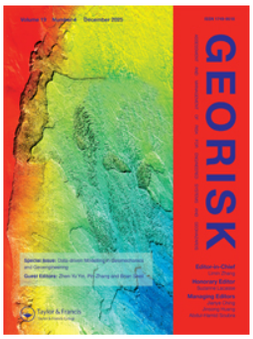

Georisk: Assessment and Management of Risk for Engineered Systems and Geohazards

ISSN: 1749-9518 (Print) 1749-9526 (Online) Journal homepage: www.tandfonline.com/journals/ngrk20

How to enrich training data for machine learning-based landslide hazard prediction with spatio-temporal precipitation information?

Ann-Kathrin Edrich, Anil Yildiz, Ribana Roscher & Julia Kowalski

To cite this article: Ann-Kathrin Edrich, Anil Yildiz, Ribana Roscher & Julia Kowalski (28 Jan 2026): How to enrich training data for machine learning-based landslide hazard prediction with spatio-temporal precipitation information?, Georisk: Assessment and Management of Risk for Engineered Systems and Geohazards, DOI: 10.1080/17499518.2026.2616779

To link to this article: https://doi.org/10.1080/17499518.2026.2616779

GEORISK
https://doi.org/10.1080/17499518.2026.2616779

Taylor & Francis
Taylor & Francis Group

How to enrich training data for machine learning-based landslide hazard prediction with spatio-temporal precipitation information?

Ann-Kathrin Edrich [a], Anil Yildiz [a], Ribana Roscher [b] and Julia Kowalski [a]

[a]Methods for Model-based Development in Computational Engineering, RWTH Aachen University, Aachen, Germany; [b]Institute of Geodesy and Geoinformation, Machine Learning in Agriculture, University of Bonn, Bonn, Germany

ABSTRACT

Landslide hazard maps indicate the spatio-temporal likelihood of landslide occurrence based on the prevailing spatial precipitation patterns. In order to generate precipitation-informed hazard maps by means of Machine Learning, we need to gather precipitation information for both landslide and non-landslide sites. For landslide locations, precipitation data associated with the initiation of the events at these sites is used. For the non-landslide locations, precipitation data is typically sampled randomly in both space and time from a precipitation database. To ensure that suitable precipitation values are sampled even when there are fewer non-landslide locations where representative random sampling may not be feasible, we test three approaches to assign precipitation values in a less random manner. As a case study, we examine the shallow landslide hazard associated with the intense rainfall event in Switzerland in August 2005. We evaluate the effectiveness of the three approaches by analysing the variation in spatial hazard distribution and the overall size of hazardous areas across the daily hazard maps produced under different precipitation conditions as well as the temporal rate of the observed changes. We conclude that probabilistically determined precipitation values offer a promising alternative to enrich non-landslide locations with precipitation-information in landslide hazard prediction.

Abbreviations: EWSs: early warning systems; ML: machine learning; AOI: area of interest; SHIRE: susceptibility and hazard mapping framework; SWRC: soil water retention curve; RF: random forest; LUCAS: land use/coverage area frame Survey; NN: neural network; AUC: area under the curve; ROC: receiver operating characteristics

ARTICLE HISTORY
Received 5 June 2025
Accepted 7 January 2026

KEYWORDS
Landslides; hazard prediction; random forest; susceptibility mapping; natural hazards

1. Introduction

Landslides impact population, infrastructure and environment worldwide (Emberson, Kirschbaum, and Stanley 2020; Miyagi 2021). They are mainly triggered by intense precipitation (Bogaard and Greco 2018; Piciullo, Calvello, and Mauricio Cepeda 2018), seismicity or anthropological influences (Turner 2018). The occurrence of precipitation as well as its total amount and intensity are not uniformly distributed over space and time. Based on this highly-varying spatio-temporal precipitation characteristics, a non-uniform distribution of landslide hazard in space and time can be assumed. From this, we conclude that landslide susceptibility mapping, i.e. the time-independent assessment for landslide occurrence (Vasu et al. 2016), which does not take the spatio-temporal changes of triggering conditions into considerations, is not often not sufficient to properly assess the potential for landslide occurrence. Landslide hazard prediction on the other hand is the temporal extension to landslide susceptibility mapping, which allows the prediction of the spatial distribution of the hazard over time. This can form the foundation for early warning systems (EWSs) which can be used for the focussed implementation of hazard mitigation measures (Piciullo, Calvello, and Mauricio Cepeda 2018).

In recent years, Machine Learning (ML) has taken on an increasingly prominent role in landslide susceptibility mapping together with increasing amount of open access landslide inventories (Mastrantoni et al. 2023). Even though the spatio-temporal characteristic of landslides has been widely acknowledged (Tonini and Cama 2019), temporal dependencies are rarely considered in ML-based landslide susceptibility

CONTACT Anil Yildiz yildiz@mbd.rwth-aachen.de Methods for Model-based Development in Computational Engineering, RWTH Aachen University, Schinkelstr. 2, 52062 Aachen, Germany

This article has been corrected with minor changes. These changes do not impact the academic content of the article.

assessments (Dahal et al. 2024; Liu et al. 2022; Nocentini et al. 2023). Providing a joint spatial and temporal assessment poses a challenge due its interdisciplinary and highly uncertain nature (Guzzetti et al. 2020; Thiebes and Glade 2018). Frequently conducted time-dependent investigations of landslide activity include, for example, the monsoon season (e.g. Kashyap, Chandra Pandey, and Ranjan Parida 2021; Sudani, Patil, and Kolekar 2021) or El Nino (e.g. Emberson, Kirschbaum, and Stanley 2021; Vilímek et al. 2013).

As described by Reichenbach et al. (2018), parameters typically included in ML-based landslide susceptibility mapping belong to the domains of (1) morphology (2) geology, (3) land cover, (4) hydrology and (5) others (see also Conforti et al. 2014; Dang et al. 2019; Edrich et al. 2024; Ishibashi 2023). Parameters from all of these domains change to some degree over time (McColl 2015). To define the parameter(s) to focus on when performing time-dependent landslide hazard prediction, two considerations can be applied: (1) time scale for relevant, large scale changes of the parameter to occur and (2) the relevance of the change to landslide initiation. Large scale changes of some parameters such as topography and related altitude and slope angle typically unfold over very large time scales while others can change within minutes or hours such as meteorological parameters. Some parameters, for example, land use can be expected to show relevant change between 1 to 10 years (Van Westen, Castellanos, and Kuriakose 2008). The timeliness should be considered when searching data sources to perform landslide hazard prediction. However, time-dependent hazard prediction relies on parameters which can change significantly over a short period of time and are directly associated with landslide initiation in response to triggering events. Precipitation is a well known landslide trigger (Bogaard and Greco 2018; Li et al. 2022; Piciullo, Calvello, and Mauricio Cepeda 2018). The precipitation conditions vary in orders of hours and can therefore cause the slope hydrology to also change within hours or days, depending on the size of the catchment (Van Westen, Castellanos, and Kuriakose 2008). This quick response of the subsurface to the occurrence of precipitation and its importance for landslide initiation makes precipitation as a meteorological parameter a suitable feature for time-dependent landslide hazard prediction. If precipitation is integrated into landslide susceptibility studies, it is mostly as a time-independent parameter such as average or maximum precipitation over a specified region and time-interval (e.g. Dang et al. 2019; Edrich et al. 2024; Zhang et al. 2020). The integration of precipitation as a time-dependent parameter into the ML-based hazard prediction process is a natural extension of the established set of time-independent environmental features, due to the increased availability of precipitation data with a high temporal resolution (Panagos et al. 2017) which allow the conduction of increasingly complex precipitation-based investigations. It is important to consider that maps derived from these time-dependent parameters are only valid as long as the information of all time-dependent parameters is valid. As soon as any dataset containing a time-dependent parameter is updated with new measurements or predictions, the previously derived map is outdated and a new map has to be produced which includes the updated data (see Fell et al. 2008). Many studies discussing landslide EWSs take antecedent precipitation into account (Guo et al. 2025), however, the time interval which they consider varies significantly from 2 days (Lee et al. 2021) to several weeks (Vasu et al. 2016). Lee et al. (2021) argue that the choice of a suitable time interval depends on the landslide type and, therefore, choose a 72 h interval for their study on shallow landslides due to the shallowness of the failure plane. Antecedent precipitation is often integrated as a proxy for soil moisture information, which is not generally available and hard to generalise (Frattini, Crosta, and Sosio 2009; Ma et al. 2014). The effect of antecedent precipitation depends on various environmental parameters such as the heterogeneity of the soil in terms of strength and permeability and the regional climate (Aleotti 2004). As the subsurface conditions before the occurrence of a triggering event heavily depend on the overall climatological conditions, e.g. wet or dry periods or the influence of different seasons, some studies address this variability by adapting the way rainfall is handled depending on the prevailing conditions (e.g. Jordanova et al. 2020; Melillo et al. 2015).

Landslide EWSs are often based on the monitoring of representative parameters for slope stability (Casagli et al. 2021). Historically, the most commonly implemented EWSs relies on the definition and methodical application of precipitation thresholds, e.g. Segoni et al. (2015), Harilal et al. (2019), Chikalamo et al. (2020), Uwihirwe, Hrachowitz, and Bogaard (2020), Yuniawan et al. (2022) and Oguz et al. (2024). This procedure is based on the observation that landslides occur after exceeding a threshold of duration, intensity or total amount (Caine 1980; Sidle and Ochiai 2006). Thresholds can either be derived through empirical analysis of historic precipitation records or physics-based modelling (Segoni, Piciullo, and Luigi Gariano 2018; Sun et al. 2022). Physical modelling of thresholds is difficult to apply to large scale areas as they are computationally expensive and they require detailed information on the subsurface which is typically hard to obtain (Tehrani et al. 2022; Vasu et al. 2016). Empirical analysis is an

effective tool to investigate large areas (Guzzetti et al. 2007), however they are subjective with respect to the chosen representation of the precipitation condition (Palladino et al. 2018). EWSs that are based on rainfall parameters alone do not take into account geomorphological and other heterogeneous environmental properties of the area of interest (AOI). Therefore, they are not suitable for spatially-focussed assessments (Palladino et al. 2018). However, some studies such as Segoni et al. (2015) and Lagomarsino et al. (2013) subdivide the AOI into more homogeneous segments and determine thresholds for each segment individually to account for spatially-varying prerequisites for sliding.

Guzzetti et al. (2020) found in their review of implemented threshold-based landslide EWSs that most of them were implemented for short-term, small-scale monitoring. ML allows investigation of landslide hazard on various time frames and with its mapping unit-based determination of landslide hazard allows a higher spatial resolution than conventional threshold-based approaches. While most EWSs are restricted to geomorphologically homogeneous areas, ML-based hazard prediction typically considers several parameters from various domains directly for determining landslide hazard under specific precipitation conditions (van Natijne, Lindenbergh, and Bogaard 2020). As Piciullo, Calvello, and Mauricio Cepeda (2018) outline, EWSs can be assessed by effectiveness, i.e. the capability of generating the desired outcome, and efficiency, i.e. the archival of the desired outcome with minimum time and cost. The effectiveness of ML-based landslide hazard mapping will be a research topic for the upcoming years, however, it certainly has the ability to continuously produce maps in an efficient manner, especially if the ML pipeline has already been initialised. The prerequisite for applying ML for landslide hazard prediction, however, is the availability of suitable precipitation data and a landslide inventory that contains a time of occurrence for each entry (see Section 2.5.1).

The so far achieved results in this domain are promising for establishing ML as technique for landslide EWSs and hazard prediction in general in the future (Liu et al. 2022). Thirugnanam, Vinodini Ramesh, and Rangan (2020), for example, discuss the enhancement of conventional, sensor-based early warning using ML. They name two limitations of conventional sensor-based landslide EWSs: (1) potentially affected data transmission during a triggering event and (2) insufficient warning times despite recognised triggering conditions. Based on their review of different EWSs, they conclude that data-driven methods can support the reliability of such systems by providing 24h forecasts which could be used for preparations. They combine a now-casting ML model predicting parameters associated with slope failure such as moisture, pore-water pressure and displacements with a forecasting ML model predicting the respective conditions at a future point in time. Hemalatha, Vinodini Ramesh, and Rangan (2019) also combine precipitation forecast and sensor measurements to achieve a 24h prediction of the slope condition using support vector regression. Moon et al. (2019) investigate the influence of a range of ML models for their influence in the context of their proposed ML-based landslide EWS architecture based on discretised precipitation values. Ng et al. (2021) and Wang et al. (2021) integrate the maximum rolling rainfall, which Ren, Gao, and Gong (2024) extend to the maximum rolling rainfall index, as feature into their ML model. The maximum rolling rainfall describes the maximum rainfall within a specific rolling time interval, e.g. 24 h. Li et al. (2022) use the 3-day and 7-day accumulated precipitation as features in their comparison of three different ML algorithms for the generation of a global landslide hazard map. Stanley et al. (2021) present near real-time time-dependent global landslide hazard prediction based on the time-dependent parameters snow, soil moisture and antecedent precipitation using the XGBoost algorithm and thereby demonstrate the use of several time-dependent, landslide-related features for model training and prediction. This model has been applied by Biswas et al. (2022) on a regional scale. Nocentini et al. (2023) investigate the influence of different antecedent precipitation time intervals and absence locations sampling strategies for RF-based time-dependent landslide hazard prediction. They use cumulative precipitation as time-dependent parameter and use a pre-generated landslide susceptibility map as time-independent parameter in their model to highlight the influence of the time-dependent parameters. Xie et al. (2025) conducted a comprehensive analysis of clustered landslides induced by extreme rainfall in Guangdong Province, China by including twelve influencing factors. They found out that accumulated rainfall was highly influential after performing 100 different sampling analyses of factor weights.

One of the major challenges of ML-based landslide hazard prediction is the combination of the time-dependent precipitation information with the otherwise time-independent components of the process. The key step in this regard is the generation of the training dataset, which is a combination of *absence locations*, i.e. non-landslide locations, and historic landslide events, also referred to as *presence locations*. As absence locations need to be representative for the locations where no landslides occur, sampling them is a challenging task

in time-independent landslide susceptibility mapping (see Hong et al. 2019; Zhu et al. 2019). Adding a temporal component to the mapping process increases the complexity further due to the added challenge of needing to tie a time-dependent parameter, e.g. precipitation, to a time-independent absence location. For landslide locations that have a timestamp of occurrence tied to them, precipitation records can be used to introduce precipitation into the training dataset. Absence locations lack such a timestamp. There is no trivial or widely accepted solution to introduce precipitation into the training dataset.

Absence location sampling can be considered from two points of view. On the one hand, they can be considered 3-dimensional data points (longitude, latitude and time) which can be sampled independently in space and time, i.e. brute force assigning a timestamp to a physical location and deriving corresponding precipitation values from precipitation records. On the other hand, they can be regarded as 2-dimensional locations that are sampled in space only and their precipitation values introduced into the training dataset are results of assessments for representativeness of the precipitation patterns and relevance regarding landslide initiation. Stanley et al. (2021) and Li et al. (2022), for example, sample absence locations independently in space and time. Xiao et al. (2022) and Ng et al. (2021) sample absence locations which can be assumed to have experienced the same heavy rainfall events as the presence locations. Similarly, Dai and Lee (2003) sample absence locations from heavy rainfall events which they assume did not trigger landslides. Jones et al. (2021) sample random absence locations equally distributed over their 12 year observation period. This view on absence locations includes the usage of presence points as absence points if they are sampled temporally before the time of failure such as done by Liu et al. (2022) and also by Nocentini et al. (2023) for testing purposes. For a large number of absence locations, it can be assumed that random sampling in space and time leads to a representative and meaningful distribution of precipitation values. For studies using a smaller number of absence locations, the representativeness of the randomly-sampled precipitation values cannot be assumed.

There is a lack in knowledge and experience in how to enrich training data for ML-based landslide hazard prediction with spatio-temporal precipitation information. This study aims at addressing this gap by defining and testing several strategies to derive representative precipitation values based on daily accumulated precipitation data. The presented approaches are applied to the test case of precipitation-triggered shallow landslide hazard in Switzerland for the August 2005 intense rainfall event.

2. Materials and methods

2.1. Susceptibility and hazard mapping framework SHIRE

The Random Forest (RF)-based susceptibility and hazard mapping framework SHIRE (Edrich, Yildiz, and Kowalski 2023) was introduced in Edrich et al. (2024). SHIRE provides flexible implementations of the necessary steps for landslide susceptibility mapping and hazard prediction: (1) conceptualisation, i.e. the definition and setup of the study parameters, (2) preprocessing of the typically inhomogeneous geospatial data and their combination into the necessary RF input datasets, (3) RF training and map generation and (4) validation and quality control of the trained model. SHIRE was developed to facilitate and streamline landslide susceptibility mapping and hazard prediction studies by reducing the time and effort necessary. It is Python-based and its modular structure introduces flexibility with regard to its application in different AOIs, the integrated data and the desired resolution.

In this paper, SHIRE (release v2.0) is the technical foundation for generating the time-dependent hazard maps. SHIRE takes the raster input datasets introduced in Section 2.3.3 to produce the training and prediction dataset and returns the probabilities for landslide occurrence. The precipitation values according to the in Section 2.5.3 presented approaches were manually prepared and added to the training and prediction datasets. These input datasets were prepared using SHIRE based only on the time-independent features (see Section 2.3.3). SHIRE was used for model training and map generation. The returned probabilities of occurrence are then, outside of SHIRE, subdivided in 5 hazard classes: *very low* (<20%), *low* (20–39.9%), *moderate* (40–59.9%), *high* (60–79.9%) and *very high* (>80%).

2.2. Test case

Shallow landslides occur frequently in Switzerland (Lateltin et al. 2005). The spatio-temporal variability in the hazard of rainfall-triggered shallow landslides in Switzerland during the intense rainfall event of August 2005 is analysed as a test case scenario in this study. This analysis is used to investigate and assess approaches for determining precipitation values to be included in the training dataset for absence locations. This is a spatio-temporal extension of the test case used in Edrich et al. (2024). Switzerland was chosen

due to the availability of spatio-temporal landslide inventory data and high-resolution geospatial datasets. Furthermore, Switzerland displays a variety of topographic and environmental characteristics including mountainous terrain, which increases the likelihood of the occurrence of shallow landslides (Dilley et al. 2005; Lateltin et al. 2005).

The August 2005 intense rainfall event which peaked on 21 and 22 August (Beniston 2006) caused significant damage in the alpine region including Switzerland (Hilker, Hegg, and Zappa 2008; Zieher et al. 2016). It resulted in a number of casualties and about 1–2 billion Euros in infrastructural damage (Beniston 2006). For this study, we define an observation period between 16 and 29 August 2005. This observation period was chosen to capture the full range of precipitation conditions before, during and after the event. Furthermore, the observation period is suitably long with respect to the time interval in which antecedent precipitation is considered in this study. Figure 1 shows the precipitation in the AOI over the observation period starting from 18 August due to the lack of significant precipitation on the previous days. The focus of this study is the development and optimisation of the hazard prediction results during the intense rainfall event, however, we discuss also the challenge of hazard predictions under no precipitation occurrence.

SHIRE is utilised to generate hazard maps with a resolution of 50 m using precipitation values for absence locations in the training dataset that, while subjective, are representative for landslide non-occurrence and relevant for the physical triggering mechanism. The time-independent features elevation, slope angle, aspect, sand, silt and clay content, bulk density, percentage of coarse fragments, available water capacity, the parameters saturated water content, α and n of the Soil

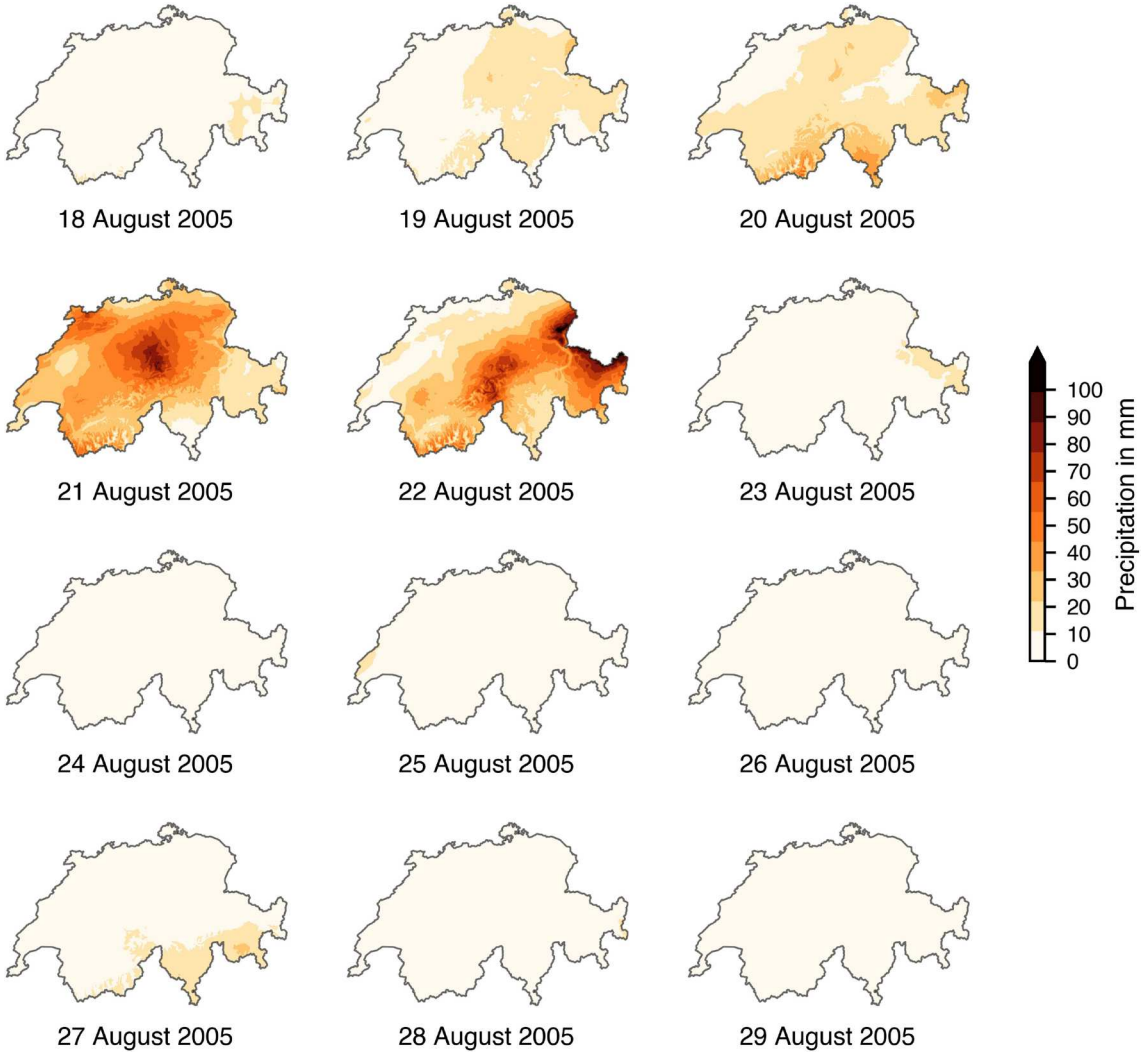

Figure 1. Precipitation in the AOI between 18 August and 29 August 2005. Swiss boundaries taken from Federal Office of Topography Swisstopo (2021).

Water Retention Curve (SWRC; Van Genuchten 1980) and tree cover density are complemented by the time-dependent 4-day accumulated precipitation feature. The choice for this time interval is discussed in Section 3.3.2. A split of 80:20 for the training and test dataset is used. The RF was set to 100 trees and a depth of 20 and the Gini impurity index is being used as splitting criterion. Additionally, using only the time-independent features but otherwise identical settings, a time-independent landslide susceptibility map is produced for reference and comparison purposes.

2.3. Data

2.3.1. Landslide inventories

The *Hangmuren* database, published by the Swiss Federal Institute for Forest, Snow and Landscape Research WSL, Mountain Hydrology and Mass Movements (2023), comprises 756 shallow landslides, recorded on 13 different dates between 1997 and 2014 (as of March 2021) through field campaigns following intense rainfall events in Switzerland (Rickli et al. 2019). Table 1 provides an overview of the temporal distribution of the landslides in the inventory. The contained landslides are spatially clustered (see Figure 2(a)) which may result from the manual compilation of the database. We extract the location and date of landslide occurrence from the *Hangmuren* database. Figure 3 shows some examples of shallow landslides in the *Hangmuren* database which occurred in the canton Grisons, Switzerland, in August 2005.

Hählen (2023) provides a landslide inventory for the Swiss canton Bern with 528 landslides which were digitised as polygons from orthophotos. For this study, we manually defined a point coordinate at the scarp of each landslide. Some landslides in the inventory are directly liked to a date of occurrence. We use only the 177 landslides in the inventory that are associated with the intense rainfall event in August 2005 for validating the time-dependent landslide hazard maps. The distribution of these landslides is illustrated in Figure 4.

Table 1. Summary of the subset of the *Hangmuren* database used for the study (Status March 2021).

Date [yyyy-mm-dd]	Number of records
1997-08-15	280
2002-09-01	106
2002-07-16	64
2002-11-14	1
2002-11-15	34
2005-08-22/23	217
2012-07-04	38
2014-07-12	2
2014-07-24	4
2014-07-28	5
2014-08-11	3
2014-11-05	2

2.3.2. Absence location sampling

Absence locations are non-landslide locations, i.e. locations where no landslides were recorded. For sampling these locations, we follow the recommendation by Hong et al. (2019) and Liu, Tang, and Huang (2023) to choose a ratio of 1:1 between presence and absence locations. Spatially, absence locations are randomly sampled based on a meshing approach. For this, we define a mesh with an equal resolution as the final hazard map and randomly sample grid cells as absence locations that have a distance of at least 50 m to a landslide location, are not associated with water bodies, are not impervious locations, and have a slope angle between 20° and 50°. These restrictions were made based on domain knowledge. This way, absence locations are sampled identically to the way it is performed for susceptibility mapping (e.g. Edrich et al. 2024), without assigning the absence locations a time-stamp. Figure 2(b) shows their spatial distribution.

2.3.3. Geospatial datasets

A total of 13 time-independent features for the ML input datasets were selected which can be expected to physically influence the stability of the subsurface or act as proxies for non-available environmental information: elevation, slope angle, aspect, sand, silt and clay content, bulk density, percentage of coarse fragments, available water capacity, the parameters saturated water content, α and n of the SWRC and tree cover density. The features were chosen based on the domain knowledge on conditioning factors and based on availability. The features cover the environmental domains of morphology, geology, land cover and hydrology (see Reichenbach et al. 2018).

Table 2 provides an overview of the datasets used, their publisher and their properties. The topographic features were derived from the digital elevation model DHM25, with a resolution of 25 m, provided by the Federal Office of Topography swisstopo (2005). The slope angle and aspect maps were derived using QGIS (QGIS Development Team 2020). Soil-related features were extracted from the Topsoil Physical Properties for Europe dataset with a resolution of 500 m which is derived from the Land Use and Coverage Area frame Survey (LUCAS) topsoil point-data (Ballabio, Panagos, and Monatanarella 2016). Information contained are percentage of coarse fragments, bulk density, available water capacity and sand, silt and clay content. Parameters of the SWRC were extracted from the 3D Soil Hydraulic Database of Europe, which is available with a resolution of 250 m (Tóth et al. 2017). Vegetation-related information is integrated through the tree cover density dataset with a resolution of 10 m

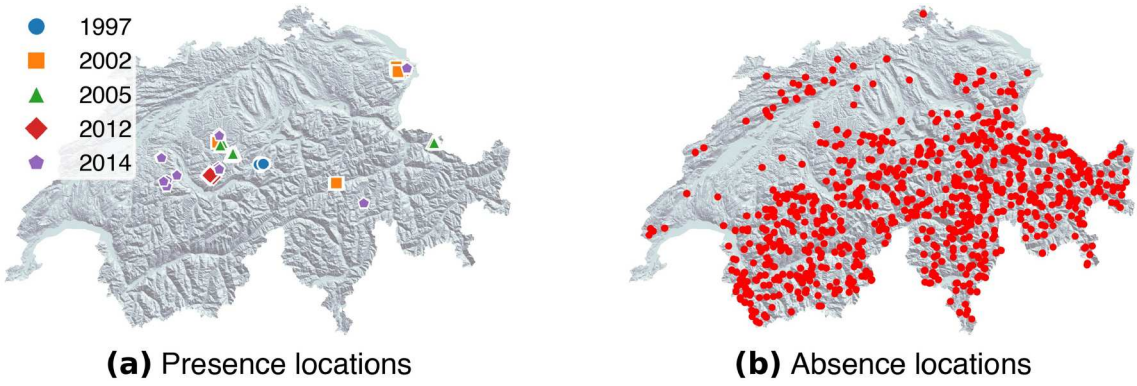

Figure 2. (a) Distribution of the presence locations given in the *Hangmuren* database by the Swiss Federal Institute for Forest, Snow and Landscape Research WSL, Mountain Hydrology and Mass Movements (2023), colour-coded by their year of occurrence (status March 2021), (b) Distribution of the sampled absence locations (red dots). Topographic basemaps derived from the DHM25 (Federal Office of Topography swisstopo 2005). Swiss boundaries taken from Federal Office of Topography Swisstopo (2021).

(Copernicus Land Monitoring Service 2018). The in Table 2 listed imperviousness and water & wetness datasets have not been used as features but were used to constrain locations to sample absence locations from (see Section 2.3.2). We work in the WGS84 coordinate reference system and therefore convert all data that are not available in this coordinate reference system to WGS84 using QGIS (QGIS Development Team 2020).

2.3.4. Precipitation data

Daily accumulated precipitation raster files from the European climatic database, hosted at University of Natural Resources and Life Sciences, Vienna, Austria between January 1950 and December 2022 with a resolution of 1 km, are used in this study (Moreno and Hasenauer 2016; Pucher 2023). We generate an accumulated precipitation time series with $\Delta t = 4$ days (i.e.

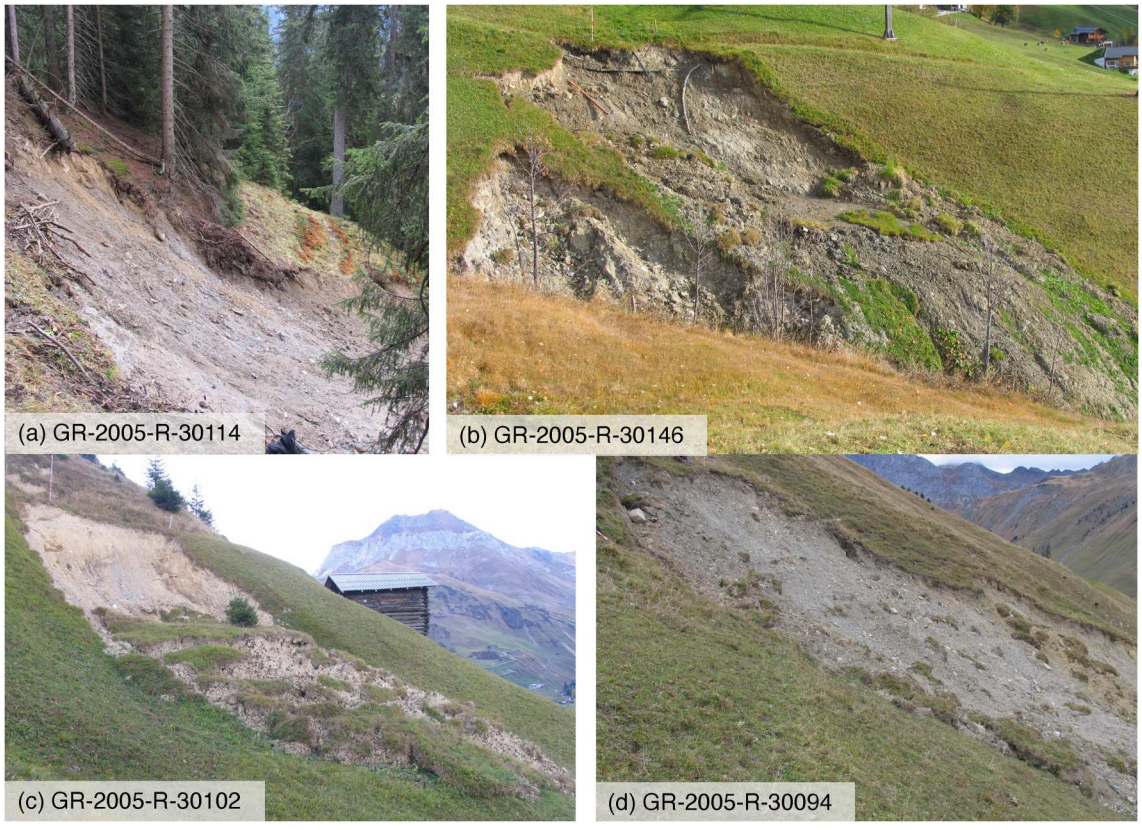

Figure 3. Exemplary images of shallow landslides taken from the *Hangmuren* database, published by the Swiss Federal Institute for Forest, Snow and Landscape Research WSL, Mountain Hydrology and Mass Movements (2023). All four landslides occurred in St. Antönien (Grisons) on the 22 August 2005.

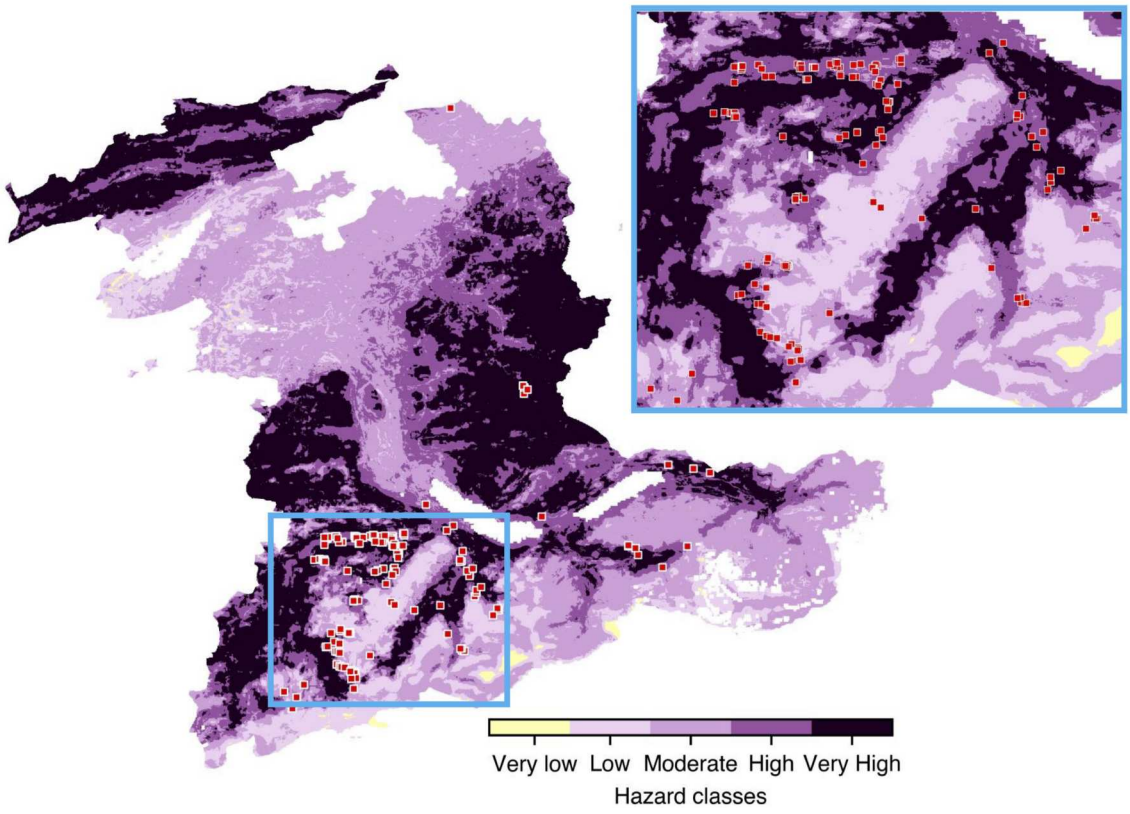

Figure 4. Distribution of the landslide inventory of the canton Bern, Switzerland (Hählen 2023). Shown are the landslides that are associated with the August 2005 intense rainfall event in red. The underlying hazard map is generated using the Probabilistic approach for 23 August 2005. The figure in the upper right corner zooms into the region marked with the blue rectangle and allows a closer look at the spatial distribution of the landslides and their respective hazard classification. Canton boundaries taken from Federal Office of Topography Swisstopo (2021).

accumulated precipitation over the current day and the three previous days) for each presence and absence location to conduct our investigations (see Section 3.3.2). The time series span the time interval between January 1950 and the landslides' individual days of occurrence for presence locations and December 2022 for absence locations.

Figure 5(a) shows the distribution of the accumulated 4-day precipitation values that are associated with landslide activity reported in the *Hangmuren* database. A

Table 2. Overview of the included datasets in the test case scenario either as features in the RF classifier input datasets or for restricting possible absence locations sampling areas.

Parameter	Unit	Dataset	Source	Resolution [m]	Extent
Elevation	m	DHM25	swisstopo	25	Switzerland
Slope angle	°				
Aspect	–				
Sand	%	Topsoil Physical Properties for Europe	ESDAC	500	Europe
Silt					
Clay					
Bulk density	g cm^{-3}				
Coarse fragments	%				
Avail. water capacity	–				
Saturated water content	cm^3 cm^{-3}	3D Soil Hydraulic Database of Europe	ESDAC	250	Europe
α (SWRC)	cm^{-1}				
n (SWRC)	–				
Tree cover density	%	High Resolution Layer: Tree Cover Density 2018		10	Europe
Imperviousness	%	High Resolution Layer: Imperviousness Density 2018		10	Europe
Water & Wetness	%	High Resolution Layer: Wetness 2018		10	Europe
Precipitation	mm	European climatic database	BOKU, Vienna	1000	Europe

Note: ESDAC: European Soil Data Centre; BOKU: University of Natural Resources and Life Sciences.

broad range of precipitation values from about 15 mm to 120 mm triggered shallow landslides. The non-even distribution of values is most likely due to the clustered nature of the *Hangmuren* database.

Considering this 4-day time interval means that precipitation since 13 August 2005 impacts the susceptibility assessment during the observation period. Figure 6 displays the accumulated 4-day precipitation over the observation period in the AOI. This spatio-temporal precipitation distribution was used as precipitation feature in the prediction dataset. Comparing Figures 1 and 6 shows the impact of including antecedent precipitation, not only in terms of magnitude, but also temporal extent in which the intense rainfall event is considered important for the landslide hazard in the AOI in this study.

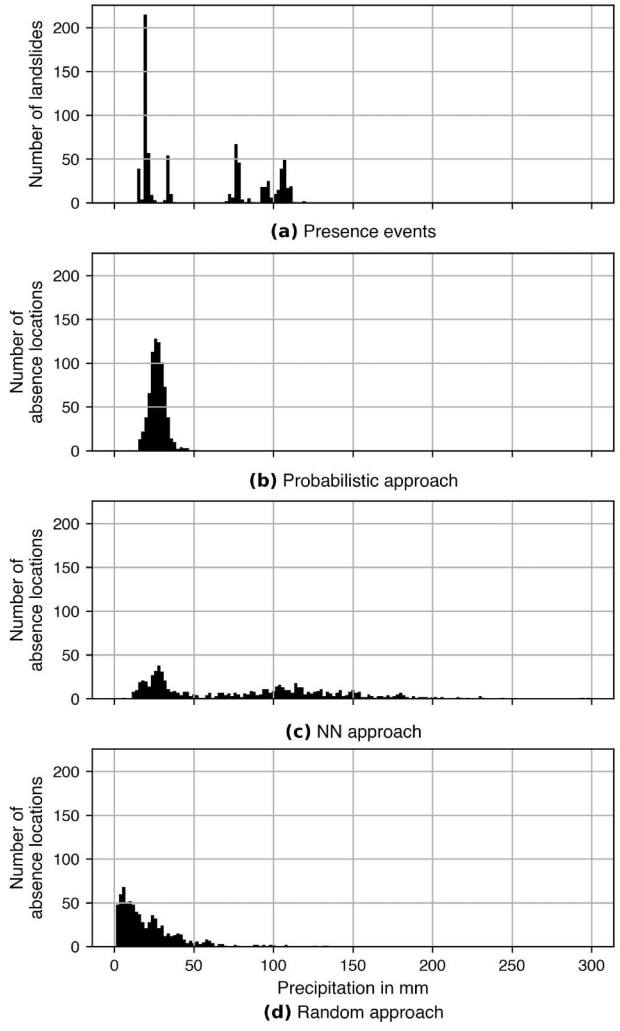

Figure 5. Distribution of precipitation values determined for (b) the Probabilistic approach, (c) the NN approach and (d) the Random approach. (a) shows the distribution of the 4-day accumulated precipitation associated with the landslide events in the *Hangmuren* database.

2.4. Combination of time-dependent and time-independent features

In some earlier studies, spatial and temporal landslide hazards were addressed independently. For example, Nocentini et al. (2023) perform time-dependent RF-based landslide hazard prediction by first preparing a time-independent categorical landslide susceptibility map and then introduce this map as a feature into the time-dependent hazard prediction. They apply this to emphasise the effect of the time-dependent features on the prediction result and to reduce the computational effort. Lee et al. (2021) separately assess the spatial and temporal probabilities of landslide occurrence and subsequently combine them through multiplication. In a similar approach, Abraham et al. (2023) generate a landslide susceptibility map and define precipitation thresholds, evaluate each independently, and then determine an overall hazard level using a predefined scheme.

In this study, the time-dependent model was trained on a training dataset consisting of time-independent features which were supplemented with the time-dependent precipitation feature. This decision is based on the assumption that many of the environmental factors used to create the susceptibility maps play a significant role in the subsurface water distribution that directly influences landslide initiation. Also, Aleotti (2004) describe that the effect of antecedent precipitation depends on various environmental factors. The procedure of assessing the spatial and temporal landslide distribution at the same time is supported also by Sidle and Ochiai (2006) who state that the influence of rainfall patterns needs to be regarded in combination with the hydrological characteristics and soil and weathered bedrock. Steger et al. (2024) furthermore claim that separating the temporal and spatial landslide hazard leads to a bias in the assigned importance of the parameters.

2.5. Precipitation values for the absence locations

2.5.1. Prerequisites

The availability of suitable precipitation data and landslide information with a date of occurrence are the necessary prerequisites for ML-based hazard prediction. Suitability of the precipitation data refers to the spatio-temporal resolution and temporal extent of the data. They need to be sufficient to capture precipitation patterns at the spatial resolution of the hazard map and the typical temporal dynamic.

The approaches presented in this study rely mostly on statistical analysis of daily precipitation time

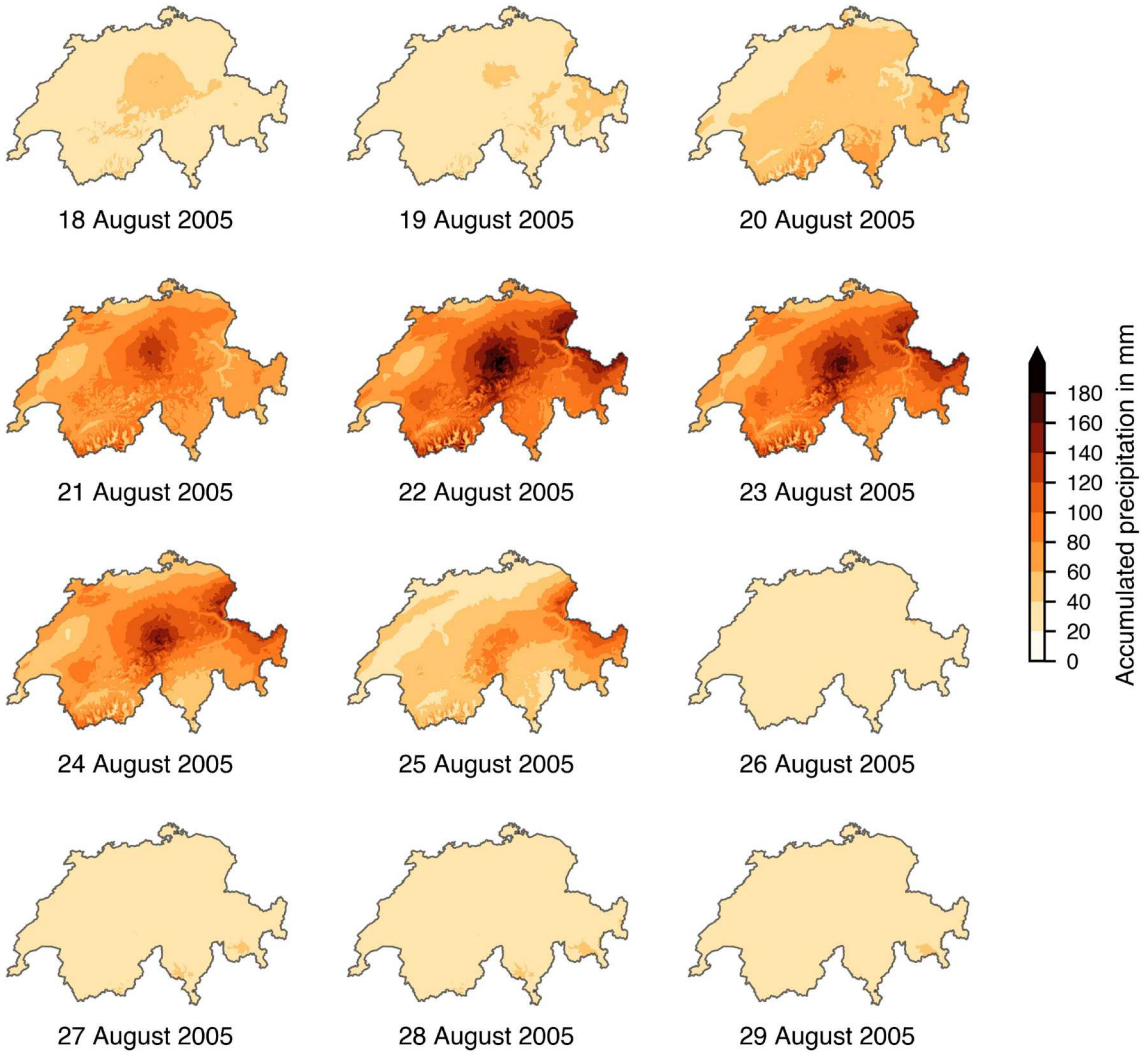

Figure 6. 4-day accumulated precipitation in the AOI between 18 August and 29 August 2005. Swiss boundaries taken from Federal Office of Topography Swisstopo (2021).

series. These time series are extracted from the precipitation data at the presence and absence locations. A suitably long observation period is required leading up to the time of occurrence of the landslides in the training dataset to achieve representativeness of the data.

The preparation of a precipitation time series $p^{(l)} = p^{(l)}(t)$ for each landslide l and $p^{(a)} = p^{(a)}(t)$ for each absence location a in the training dataset at their point position $c^{(l)}$ and $c^{(a)}$ respectively is a necessary step before applying the below presented methodology. The time series should be structured to represent the precipitation variable intended for integration into the training dataset. Here, we regard the accumulated precipitation over a given time interval Δt (see Section 2.5.2). A precipitation time series at any landslide or absence location, here now generally referred to as location x, can be described as $p^{(x)} = (p_0, p_1, \ldots, p_M)$ where $p_m = p(t_m)$ with $m \in \{0, \ldots, M\}$ are the individual instances of the time series, e.g. here, corresponding to daily precipitation values. When using accumulated precipitation values $\tilde{p}_n$ over time interval Δt, e.g. in this study $\Delta t = 4$ days (see Sections 2.3.4 and 3.3.2), the resulting time series can be described as $\tilde{p}^{(x)} = (\tilde{p}_{\Delta t}, \tilde{p}_{\Delta t+1}, \ldots, \tilde{p}_M)$ where $\tilde{p}_{\Delta t+n} = \tilde{p}(\Delta t + t_n)$ with $n \in \{0, \ldots, M - \Delta t\}$. The individual accumulated precipitation values $\tilde{p}_{\Delta t+n}$ are determined as follows:

$$\tilde{p}_{\Delta t+n} = \tilde{p}(\Delta t + t_n) = \sum_{t=t_n}^{t_n+\Delta t} p_t. \tag{1}$$

This procedure needs to be performed individually for every landslide location $c^{(l)}$ with the corresponding precipitation time series $p^{(l)}$ and for every absence location $c^{(a)}$ with the corresponding precipitation time series $p^{(a)}$.

2.5.2. Choice of precipitation variable

Most precipitation threshold EWS studies employ intensity and duration as precipitation variables to define their threshold (Segoni, Piciullo, and Luigi Gariano 2018). This is reasonable, as short-term high intensity rain can be an important factor for shallow landslide initiation (Lee et al. 2021; Montrasio and Valentino 2008). Lacking precipitation data with a high temporal and spatial resolution complicates the development of a reliable model (Tiranti and Rabuffetti 2010; Vishnu et al. 2022). The accuracy of the landslide timestamps in the inventory is also important in selecting the appropriate precipitation variable.

In this study, we use cumulative daily precipitation values, as the available landslide timestamps were recorded at the daily scale. With the temporal resolution of our landslide data and the long temporal coverage our precipitation data of more than 70 years, we avoid the introduction of additional uncertainties due to assumptions to be made and the necessary combination of precipitation data from different sources by using daily accumulated precipitation instead of precipitation intensity. Furthermore, use of cumulative precipitation is consistent with many published ML-based landslide prediction (e.g. Mondini, Guzzetti, and Melillo 2023) lowering the threshold for the application of the below presented approaches to determine precipitation values for absence locations. With this variable, however, careful consideration must be given to the choice of the antecedent precipitation time interval. For instance, a short-term, high-intensity rainfall event might result in a lower cumulative precipitation value compared to several days of moderate rainfall, potentially leading to an overestimation of landslide hazard at a given point in time. In this study, we use $\Delta t = 4$ days (see Sections 2.3.4 and 3.3.2).

2.5.3. Approaches

We apply three approaches to determine precipitation values for the absence locations. The Probabilistic approach and the Neural Network (NN) approach rely on empirical analysis of the precipitation time series while the Random approach is an extension of the commonly applied random precipitation sampling in space and time.

2.5.3.1. Probabilistic approach. The Probabilistic approach is based on an empirical analysis of the precipitation time series at presence locations to derive a manually defined precipitation probability threshold. This threshold represents the exceedance probability for landslide-triggering precipitation amounts and is calibrated by determining the likelihood that precipitation exceeds the amounts associated with landslide events in the training dataset. It is assumed to be representative of the necessary precipitation amount for landslide initiation in the area where the recorded landslides occurred.

This threshold is then applied to the precipitation time series at absence locations to determine the precipitation amount to be included in the training dataset. Specifically, the precipitation amount corresponding to the derived exceedance probability threshold is identified.

The individual steps for deriving the exceedance probability threshold from the time series of presence locations are as follows:

First, the precipitation patterns at the presence sites in the landslide inventory need to be analysed. Each landslide event l can be characterised by a position $c^{(l)}$, a time of occurrence $t^{(l)}$ and a precipitation amount $\tilde{p}(t^{(l)})$ which is associated with its failure. Assuming that for position $c^{(l)}$ a precipitation time series $\tilde{p}^{(l)}$ is available, the following steps need to be taken for every landslide in the inventory:

(1) Generate a probability density distribution of $\tilde{p}^{(l)}(t < t^{(l)})$ starting from the onset of the available precipitation data. In the case of this study, this is 01/01/1950.
(2) Identify the bin $i^{(l)}$ with the associated precipitation $\tilde{p}_{i^{(l)}}$ in the probability density distribution for which $\tilde{p}_{i^{(l)}} = \tilde{p}(t^{(l)})$.
(3) Sum over all bins to the right of $i^{(l)}$:

$$P^{(l)}(\rho_j, i^{(l)}) := \sum_{j>i^{(l)}} (w \cdot \rho_j) \tag{2}$$

where ρ_j is the probability density of the $j-$th bin and w is the bin width. The exceedance probability $P^{(l)}$ describes the probability that more precipitation occurs than $\tilde{p}(t^{(l)})$ at this landslide site.

The distribution of the resulting probabilities can be visualised in a histogram (see Figure 7). Around 29% of landslides were triggered by precipitation amounts very close to the maximum of observed precipitation at this location. This can be concluded as their determined exceedance probabilities are close to zero. Higher exceedance probabilities mean that a lower precipitation amount relative to the observed maximum was needed to trigger the landslides. This could be because (1) the landslides were triggered after short, high-intensity precipitation rather than prolonged medium intensity precipitation which might result in a lower accumulated precipitation amount or (2) less precipitation than

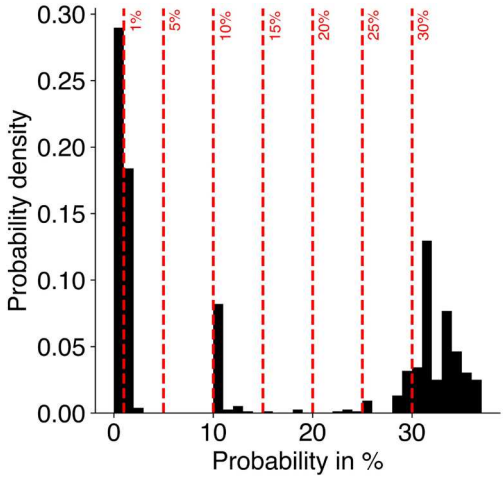

Figure 7. Distribution of exceedance probabilities of the shallow landslides in the *Hangmuren* database. The red, dotted lines mark the probability thresholds tested in this study.

usual was needed to trigger the landslide because of e.g. unusually wet conditions (see Terlien 1998). The role of precipitation intensity in triggering landslides and the consequential issue of not properly describing events caused by short, high-intensity rainfall highlights a challenge of using daily accumulated precipitation data.

Based on the histogram in Figure 7, a probability threshold P_{thres} can be defined manually. The threshold needs to be reasonably defined so that the majority of landslides are covered without the threshold being too high. This, therefore, is a subjective assessment. Due to the strong discrepancy observed in our landslide data, we furthermore test the sensitivity of the map generation to the manually determined threshold. We use the results also to support a choice of threshold. We compare the results derived when choosing thresholds 1%, 5%, 10%, 15%, 20%, 25% and 30%. Figure 8 shows the difference in the total predicted area for each hazard class in the produced landslide hazard maps for selected thresholds. We use the time-independent susceptibility map as a reference (see Section 3.1). As discussed in more detail in Section 4, we expect an increase of pixels classified as *moderate*, *high* and *very high* hazard during the most intense period of the rainfall event. For 5% and 10%, only a small change in the total area size classified as *high* and *very high* can be seen. The larger the threshold, the stronger the impact on the class distribution during the intense rainfall event. The thresholds 20% and 25% overall produce quite similar results and both adhere to the assumption that during the intense rainfall event a significant rise in the *moderate*, *high* and *very high* hazard classes should be observed and without rainfall a respective increase in *low* and *very low* hazard areas should occur. For this study, we decide for a threshold of 20%, even though it leads a slightly smaller increase in the *high* and *very high* hazard classes, as we want to credit the large number of landslides that were triggered by precipitation with a lower exceedance probability (see Figure 7).

Each absence location a is characterised by a location $c^{(a)}$. Assuming that for position $c^{(a)}$ a precipitation time series $\tilde{p}^{(a)}$ is available with the same Δt as $\tilde{p}^{(l)}$, the precipitation value $\tilde{p}_{i^{(a)}}$ to integrate into the training dataset can be derived following these steps:

(4) Generate the probability density distribution of $\tilde{p}^{(a)}$.
(5) Sum backwards over the distribution starting from the tail

$$P^{(a)}(\rho_j, i^{(a)}) := \sum_{j>i^{(a)}} (w \cdot \rho_j) \tag{3}$$

to determine bin $i^{(a)}$ for which

$$i^{(a)} := \max\{i^{(a)} : P^{(a)} \leq P_{\text{thres}}\}. \tag{4}$$

(6) Integrate the corresponding precipitation value $\tilde{p}_{i^{(a)}}$ into the training dataset for absence location a.

Extracting precipitation values from the absence location precipitation time series corresponding to the Probabilistic approach results in the distribution displayed in Figure 5(b). This approach leads to 4-day accumulated precipitation values between about 10 mm and 52 mm for the majority of absence locations with only few having significantly lower or higher values. In comparison to the presence locations' precipitation values, they, therefore, are in a similar range as the low to medium triggering precipitation values.

2.5.3.2. NN approach. The NN approach is almost identical to the Probabilistic approach. It requires the same initial steps (1), (2) and (3). However, instead of manually defining a single threshold based on all landslides, a ML model, here a NN, is trained. This model uses the time-independent environmental features of the training dataset to predict probability thresholds for each absence location a individually. The predictions are based on the commonalities of the absence locations with the presence locations, allowing us to derive $P^{(a)}_{\text{thres}}$. Then, for each absence location a, step (4) is conducted, followed by (5) with the respective $P^{(a)}_{\text{thres}}$ to determine bin $i^{(a)}$ so that

$$i^{(a)} := \max\{i^{(a)} : P^{(a)} \leq P^{(a)}_{\text{thres}}\}. \tag{5}$$

Just as with step (6) above, the corresponding precipitation value $\tilde{p}_{i^{(a)}}$ can be integrated into the training dataset for absence location a.

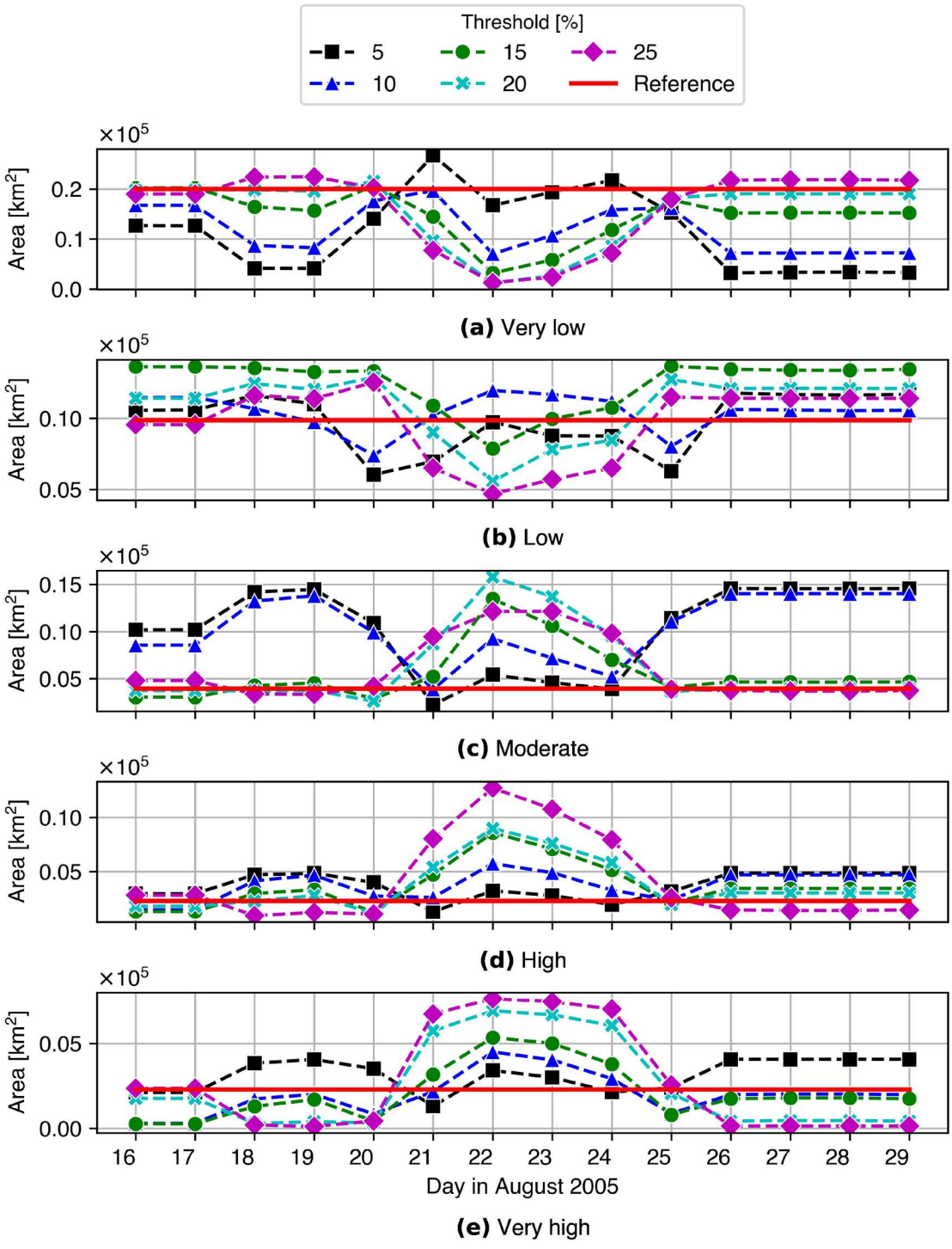

Figure 8. Comparison of the total area size of each hazard class for each day of the observation period, depending on the chosen threshold for the Probabilistic approach. The red line marks the time-independent reference susceptibility map (see Section 3.1).

Extracting precipitation values from the absence locations' precipitation time series corresponding to the exceedance probabilities predicted by the NN results in the distribution shown in Figure 5(c). These values are distributed over a range of about 5 mm to almost 232 mm and therefore cover the whole range of values in which also the landslides in the *Hangmuren* database occurred. This approach results in much more widespread precipitation values compared to the Probabilistic approach.

2.5.3.3. Random approach. The Random approach is an adaptation of the common random space-time absence location sampling strategy for a smaller number of absence locations. Investigating the precipitation time

series of the presence and absence locations reveals significantly more dry than wet days. Therefore, the precipitation time series of the absence locations are cleaned from days below a pre-defined precipitation amount threshold T so that $\tilde{p}^{(a,\geq T)} = \{\tilde{p}_j^{(a)} \mid \tilde{p}_j^{(a)} \in \tilde{p}^{(a)}, \tilde{p}_j^{(a)} \geq T, j \in \{\Delta t \ldots, M\}\}$. We investigated the impact of the choice of threshold T by comparing the resulting maps when choosing 1 mm, 10 mm, 20 mm, 30 mm, 40 mm, 50 mm, 60 mm, 70 mm and 80 mm as 4-day accumulated precipitation threshold. Note that with increasing size of the considered antecedent precipitation time interval Δt, the number of instances which are removed decreases. If, due to a long antecedent precipitation interval, no days are removed, it equals the random space-time sampling commonly applied by previous studies. Among the remaining instances, the precipitation value for the specific absence location is sampled randomly. This can be repeated for all absence locations in the training dataset. As, apart from the removal of the elements below threshold T of the time series, no changes are made, the random sampling still adheres to the original distribution of the precipitation values $\geq T$ and their corresponding frequency pattern.

Figure 9 shows the total predicted area for each hazard class in the produced landslide hazard maps for selected thresholds. We included the time-independent prediction as a reference (see Section 3.1). The most prominent observation is that during the intense rainfall event especially for the *very low*, *low* and *high* hazard classes for all thresholds the total area is close to the area derived from the reference. Based on the same line of argumentation as for the Probabilistic approach, high thresholds such as 60 mm are not considered. The low thresholds lead to reasonable results. Based on these observations, we chose the 1 mm threshold as this allows the inclusion of the maximum number of entries of the precipitation time series data.

The distribution of the absence locations' precipitation values derived through the Random approach is shown in Figure 5(d). Here, the randomly sampled values are mostly below 50 mm, and, therefore, mostly lower than the values of the other approaches. This is to be expected as intense rainfall events are comparably rare and most days with precipitation >0 mm show also only little rain.

3. Results

3.1. Time-independent reference map

To demonstrate the impact of the temporal characteristic of precipitation, we compare the obtained results to a time-independent landslide susceptibility map (see Figure 10). The map illustrates the spatial distribution of predicted landslide susceptibility, categorised in hazard classes which indicate the likelihood of landslide occurrence from *very low* to *very high*. As would be expected, in the majority of Switzerland, especially in flat terrain, the likelihood of occurrence is *very low*. *Very high* likelihood aligns with steep terrain. This map is used as a reference map in this study.

3.2. Comparison of generated maps

Figure 11 illustrates the total size of the area categorised into the individual hazard classes for each day of the observation period for the three approaches. The Probabilistic approach causes the strongest spatio-temporal changes with a strong increase in total size of the *very high*, *high* and *moderate* hazard classes during the intense rainfall event and the consecutive days, which are still affected by the strong rainfall. The results for the Random approach are similar in pattern, leading, however, to significantly reduced magnitude of changes in the classification of the AOI. Overall, the NN approach shows the lowest sensitivity to the occurring precipitation conditions. For the days before and after the heavy rainfall event, the three approaches show varying behaviour for the different hazard classes. All three approaches show almost no areas with *very high* hazard before and after the event. The other classes show more variations between the approaches. For example, before the event, the Random approach has a larger area of *very low* hazard while the Probabilistic and NN approach have more *low* hazard areas before the event. In the days after the event, the variation in total size of the different classes are smaller due to the consistent lack of significant precipitation. The NN and Random approaches show hardly any area of *high* hazard after the event and the Random approach does also not predict any areas of *moderate* hazard.

Figure 11 only allows conclusions on the total size of the area assigned a certain hazard class, while Figures 12–14 illustrate their spatial distribution. They show landslide hazard maps of selected dates within the period of observation which display different precipitation conditions. The maps of all three approaches show spatio-temporal sensitivity, i.e. the distribution of the hazard classification of the AOI varies over time in response to the spatial precipitation conditions. However, each approach results in a unique characteristic of the spatial distribution of classes. For all three approaches, similar to the reference, the *very high, high* and *moderate* classified areas focus on the area of

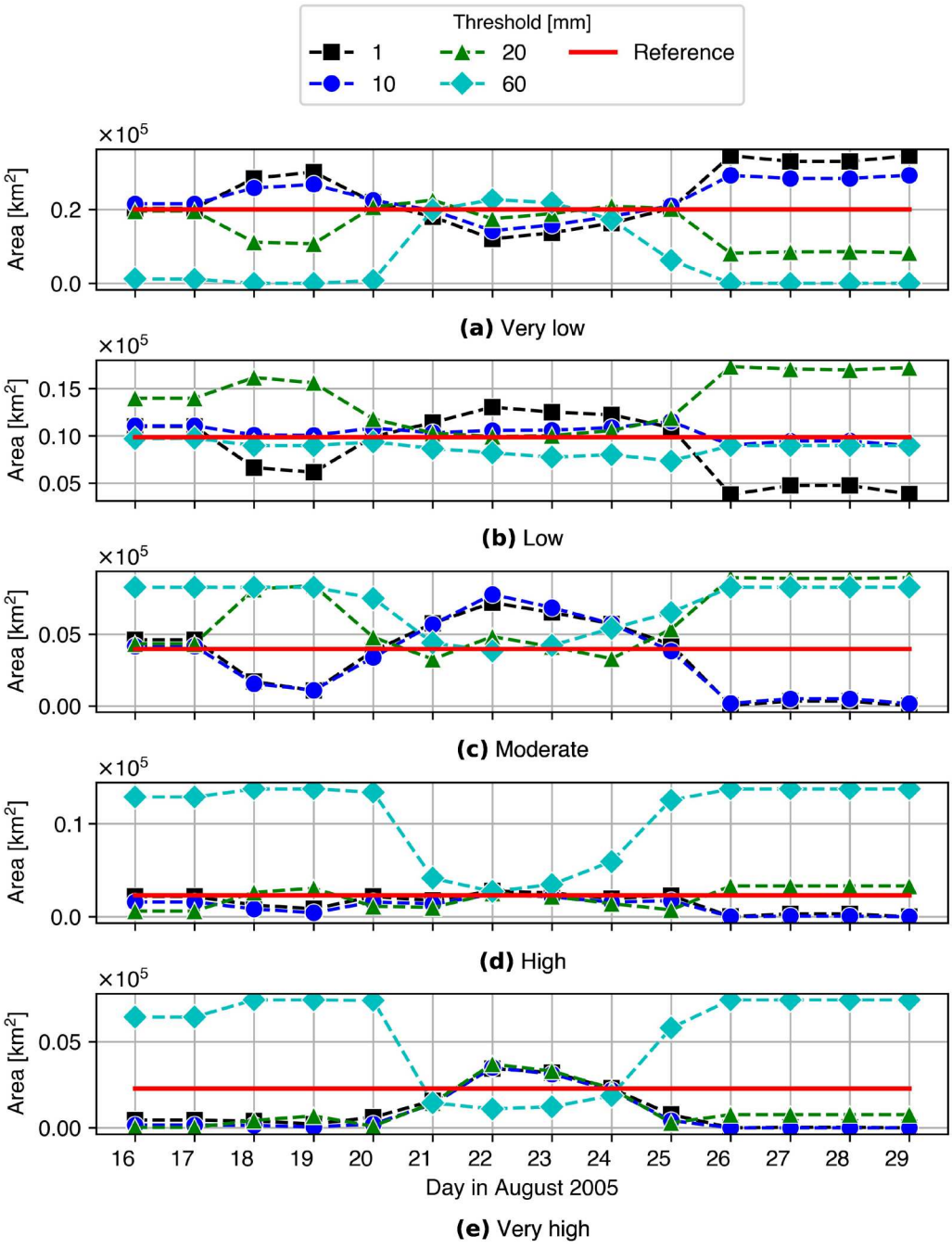

Figure 9. Comparison of the total area size of each hazard class for each day of the observation period, depending on the chosen threshold for the Random approach. The red line marks the time-independent reference susceptibility map (see Section 3.1).

strong topography, the most prominent spanning in a belt from the north-east to the south-west.

The Probabilistic approach over the entire observation period shows a stronger and more wide-spread hazard of higher classes than the other two approaches. The NN approach, as already described above, varies least, however, still shows a reasonable development in accordance with the changing precipitation conditions. The Random approach leads to results similar in pattern to the Probabilistic approach, however, the development is less distinct.

3.3. Validation

3.3.1. Assessment of the time-dependent landslide hazard maps

The test dataset, domain knowledge and "hindcast" (Guzzetti et al. 2020) are used to assess the validity of the individual approaches for landslide hazard prediction. The Brier score of all trained models is better or equal to 0.05 and the Logarithmic loss of all models is better than 0.18. These values give the impression of

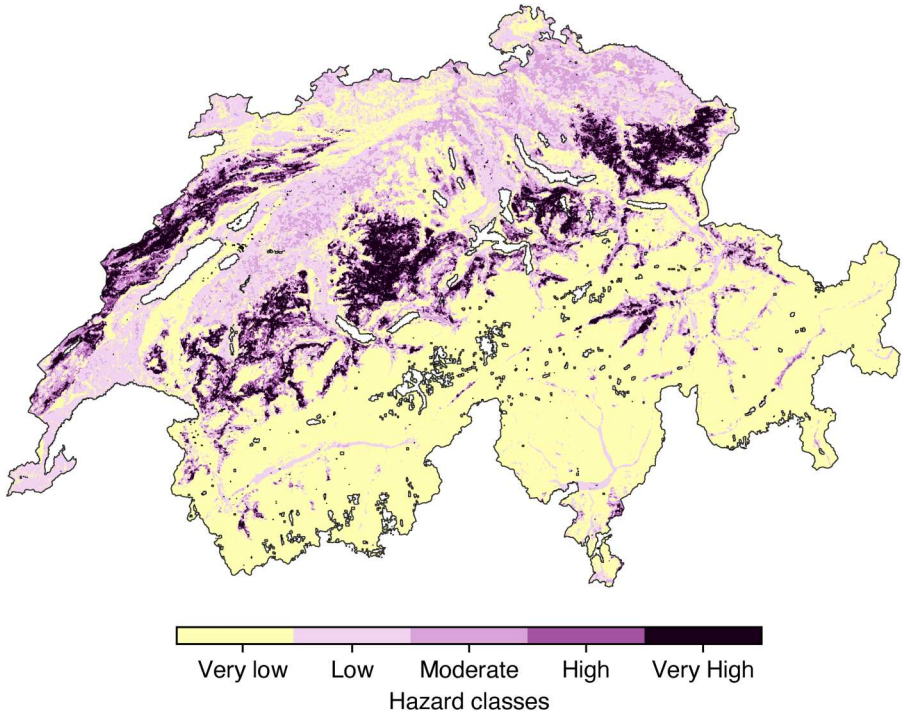

Figure 10. Time-independent landslide susceptibility map of Switzerland generated using the time-independent features of this study. The susceptibility is displayed as classes of likelihood of occurrence ranging from *very low* to *very high* with the respective colour-coding. The white, outlined areas in the the map mark areas for which a prediction was not possible due to missing data. Swiss boundaries taken from Federal Office of Topography Swisstopo (2021).

high quality models. However, it must be assumed that the quality here is also significantly overestimated due to the clustered nature of the presence instances in the training dataset.

"Hindcast" refers to the application of a trained model to a past intense rainfall event and the comparison of the predicted hazard to the observed landslides of this event (Guzzetti et al. 2020). It provides an indication of the plausibility of the distribution of the predicted hazardous areas similar to the test dataset but allows no conclusions on other aspects of the time-dependent maps such as the plausibility of the rate of change in the total size of hazardous area and the development in areas without landslides recorded in the multi-year inventory. For hindcasting, we use the landslides in the canton Bern (see Figure 4; Hählen 2023). Figure 15 shows the number of landslides given in this inventory that are assigned to the different hazard classes for the entire observation period for all three applied approaches. The development of the landslide locations' hazard classification and the development of the total area classified as a specific hazard illustrated in Figure 11 are similar in pattern.

We expect that during the intense rainfall event, ideally, the landslides that were triggered are located in areas that are of *high* or *very high* hazard. For the Probabilistic approach, this expectation is fulfilled. The NN approach does not fulfill this requirement with the majority of landslides occurring in *low* and *very low* hazard areas. For the Random approach most landslides were triggered in *high* hazard areas and fewer were triggered in *moderate* or *very high* hazard areas. These relations are also visible in Figure 16. Figure 15 furthermore shows the development of the hazard classification of the landslide locations over the observation period. Ideally, before and after the triggering event, the classification of the landslide locations shows lower class hazard. This tendency is visible for all three approaches.

The short-comings of the test case shall be addressed here as well, as they impact the hazard map interpretation. Especially the sub-optimal distribution of shallow landslides in the *Hangmuren* database might negatively impact the representativeness of the training dataset. The representativeness issues of the clustered landslide data also transferred to the triggering precipitation values introduced in the training dataset enhanced by the coarse spatial resolution of the precipitation data. Nevertheless, the preconditions were identical for all generated maps and therefore, it is assumed that the discussion of the validity of the individual approaches, their advantages and disadvantages is not significantly impacted. However, in Section 4 the matter will be

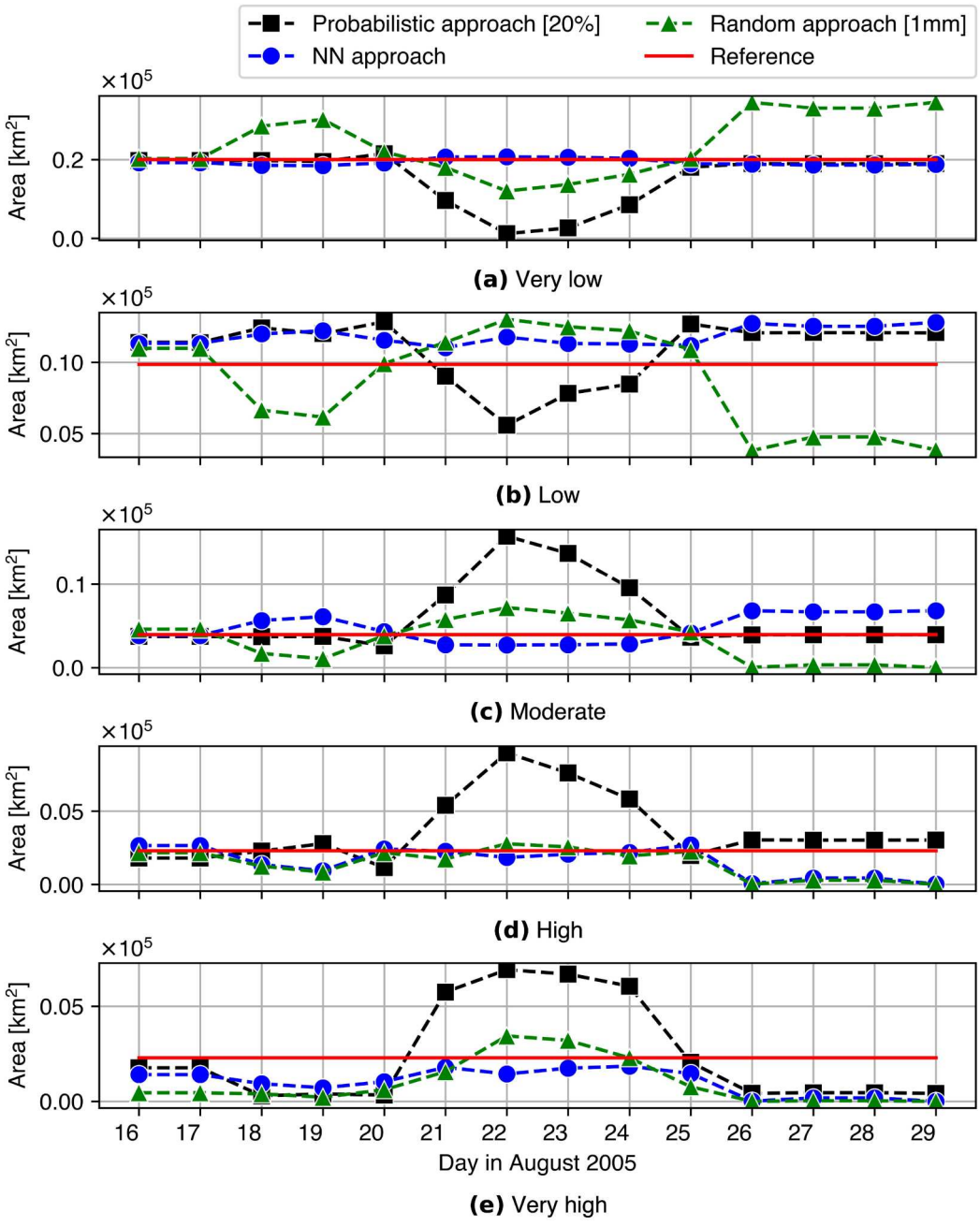

Figure 11. Comparison of the total area size of each hazard class for each day of the observation period for the three employed approaches. The red line marks the time-independent reference susceptibility map (see Section 3.1).

addressed when necessary to properly assess the validity of the approaches.

3.3.2. Choice of antecedent precipitation time interval

This study uses $\Delta t = 4$ days (i.e. the accumulated precipitation over the current day and the three previous days). The decision for this time interval is based on the evaluation and comparison of the hazard prediction results for 23 August 2005 using $\Delta t \in \{2, 3, 4, 5, 6, 7, 8\}$ days. Similarly to hindcasting as assessment of the quality of the time-dependent hazard maps in Section 3.3.1, we determine for each created hazard map with its individual applied precipitation approach and Δt the percentage of landslides reported in the Bern landslide inventory that fall into each hazard class. The results can be found in Figure 16. As we expect a high quality hazard map to predict *high* or *very high* hazard at the locations where landslides actually occurred, we base the choice of Δt on the percentage of landslides falling in those two categories. $\Delta t = 4$ days shows in both classes for all three

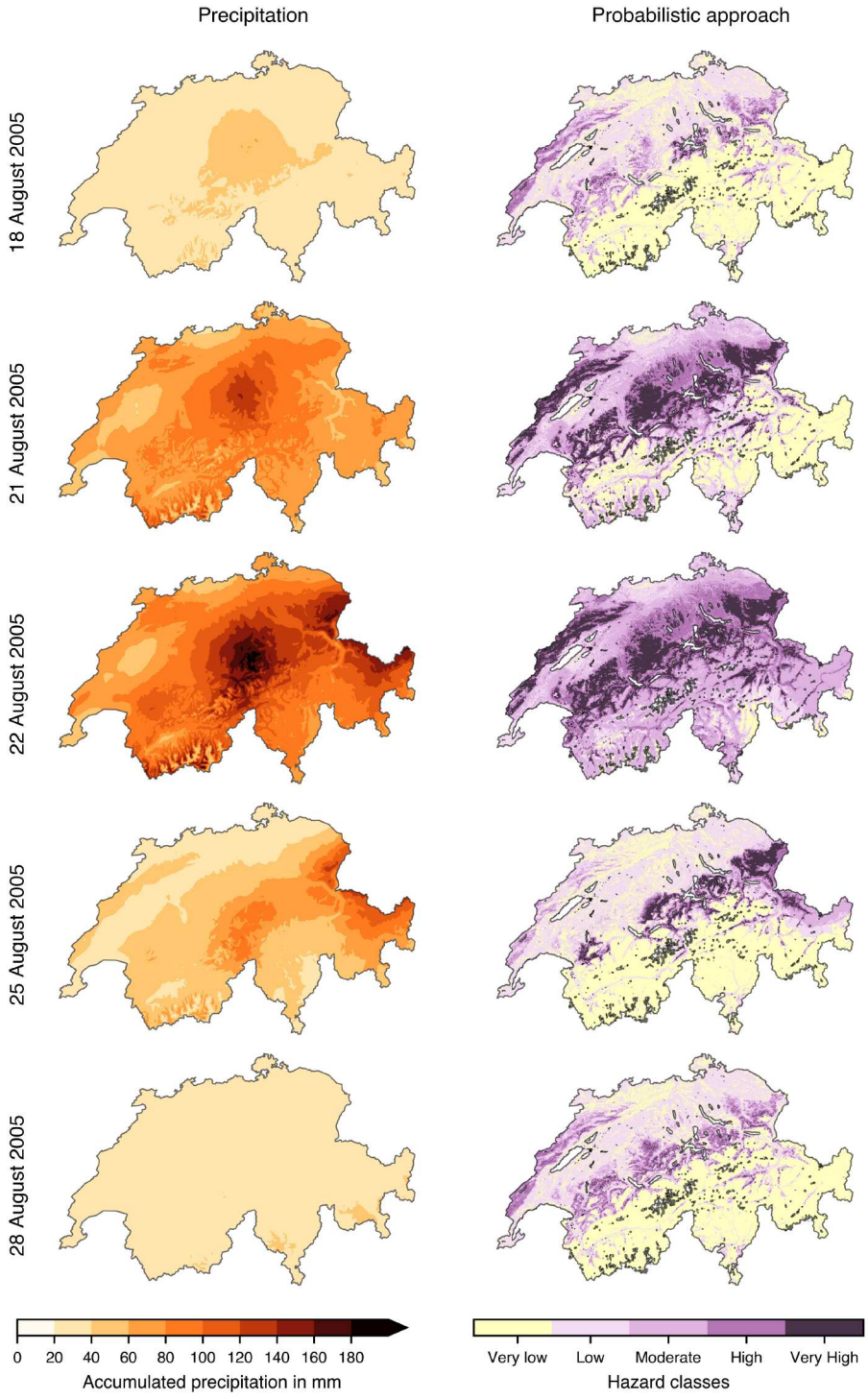

Figure 12. Illustration of the development of the hazard of shallow landslides in the AOI between 16 and 29 August 2005 based on the Probabilistic approach, showing exemplary maps of this period. The white, outlined areas indicate areas in which a prediction was not possible. For reference purposes the 4-day accumulated precipitation is provided as well. Swiss boundaries taken from Federal Office of Topography Swisstopo (2021).

approaches the highest number of landslides. From this assessment, we conclude that $\Delta t = 4$ days is a suitable antecedent precipitation time interval. However, the figure also reveals that the choice of time interval, overall, does not impact the classification result significantly.

3.3.3. Assessment of the time-independent landslide susceptibility map

SHIRE includes automatic assessment of the Logarithmic Loss, the Brier score and the Area under the Curve (AUC) of the Receiver Operating Characteristics

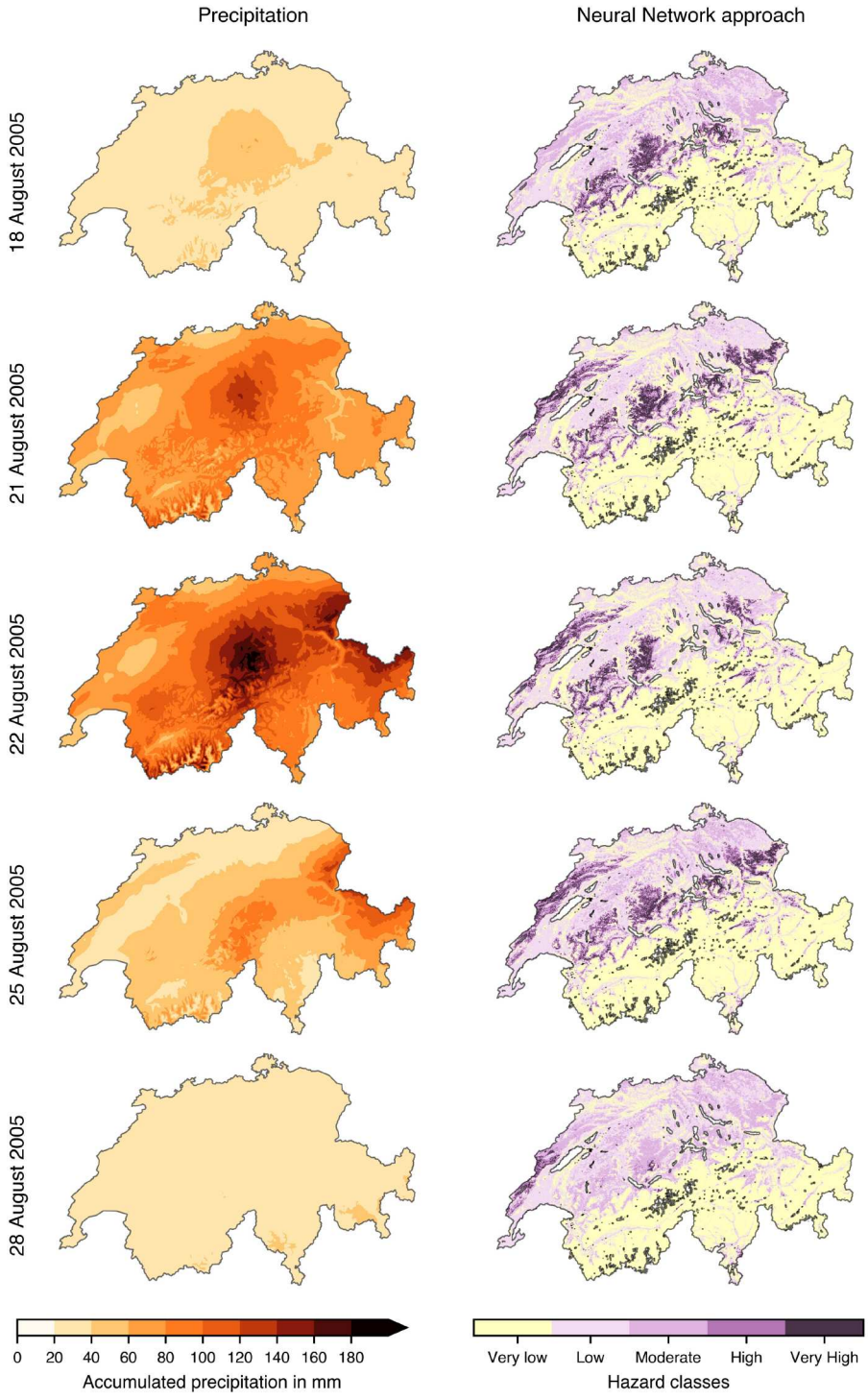

Figure 13. Illustration of the development of the hazard of shallow landslides in the AOI between 16 and 29 August 2005 based on the NN approach, showing exemplary maps of this period. The white, outlined areas indicate areas in which a prediction was not possible. For reference purposes the 4-day accumulated precipitation is provided as well. Swiss boundaries taken from Federal Office of Topography Swisstopo (2021).

(ROC) curve. For the time-independent landslide susceptibility map (see Figure 10), used as reference in this study, the Logarithmic Loss was determined as 0.2, the Brier score is 0.06 and the Area under the curve is 0.98. All of these values indicate a good model quality. However, we are aware of the weaknesses of the *Hangmuren* database used for model training with its clustered nature and therefore reduced representativeness (see Edrich et al. 2024). To assess the impact, we applied spatial thinning of the landslide

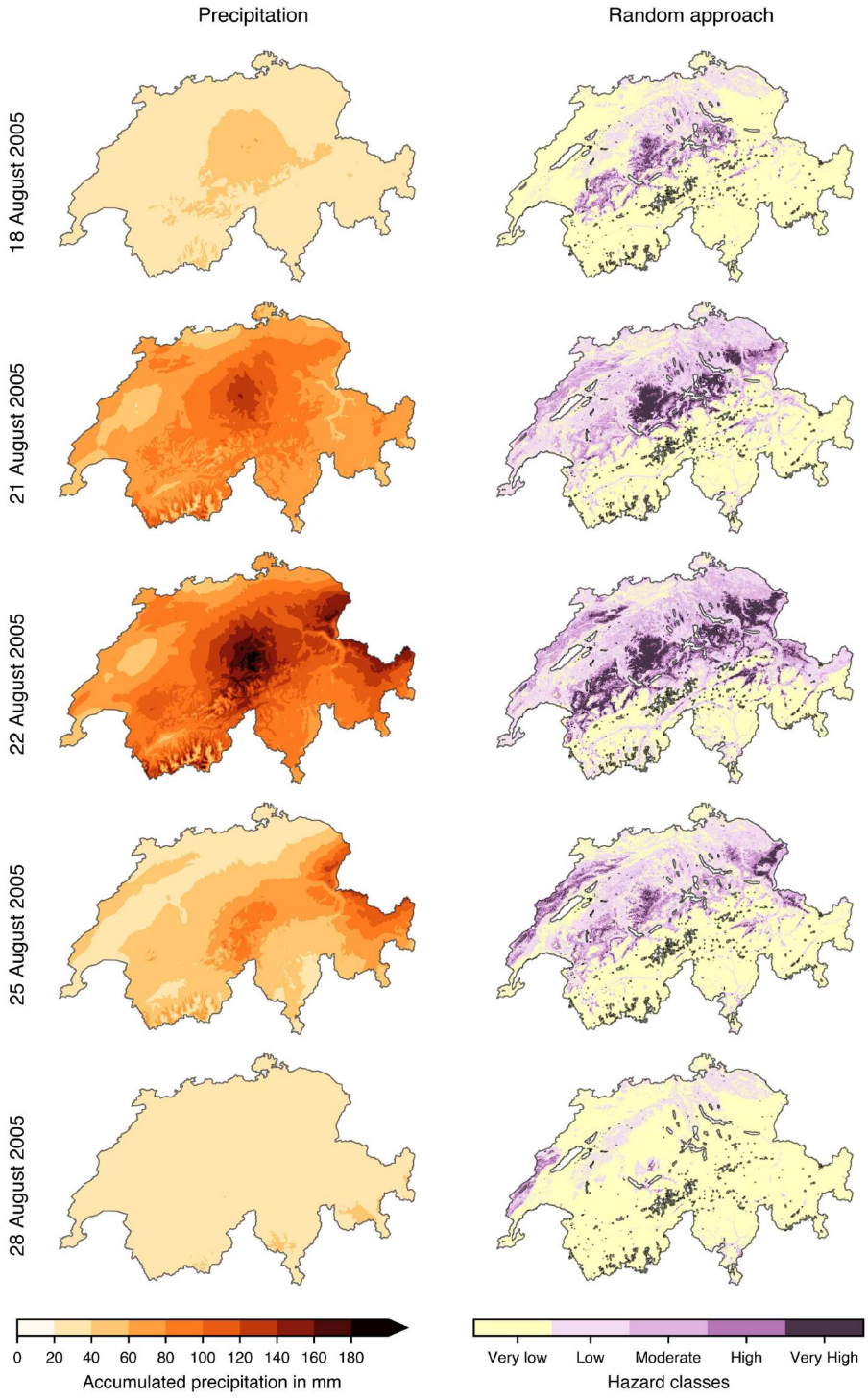

Figure 14. Illustration of the development of the hazard of shallow landslides in the AOI between 16 and 29 August 2005 based on the Random approach, showing exemplary maps of this period. The white, outlined areas indicate areas in which a prediction was not possible. For reference purposes the 4-day accumulated precipitation is provided as well. Swiss boundaries taken from Federal Office of Topography Swisstopo (2021).

locations. To retain the ratio of absence to landslide locations, we removed an equal amount of absence locations. With a 200 m minimum spacing between landslides in the training data, model predictive performance decreased only moderately (Brier score 0.08, Logarithmic Loss 0.27). However, applying 500 m minimal distance of the landslide locations revealed a larger reduction in predictive confidence, reflecting the presence of some strongly clustered areas (Brier score 0.11, Logarithmic Loss 0.35).

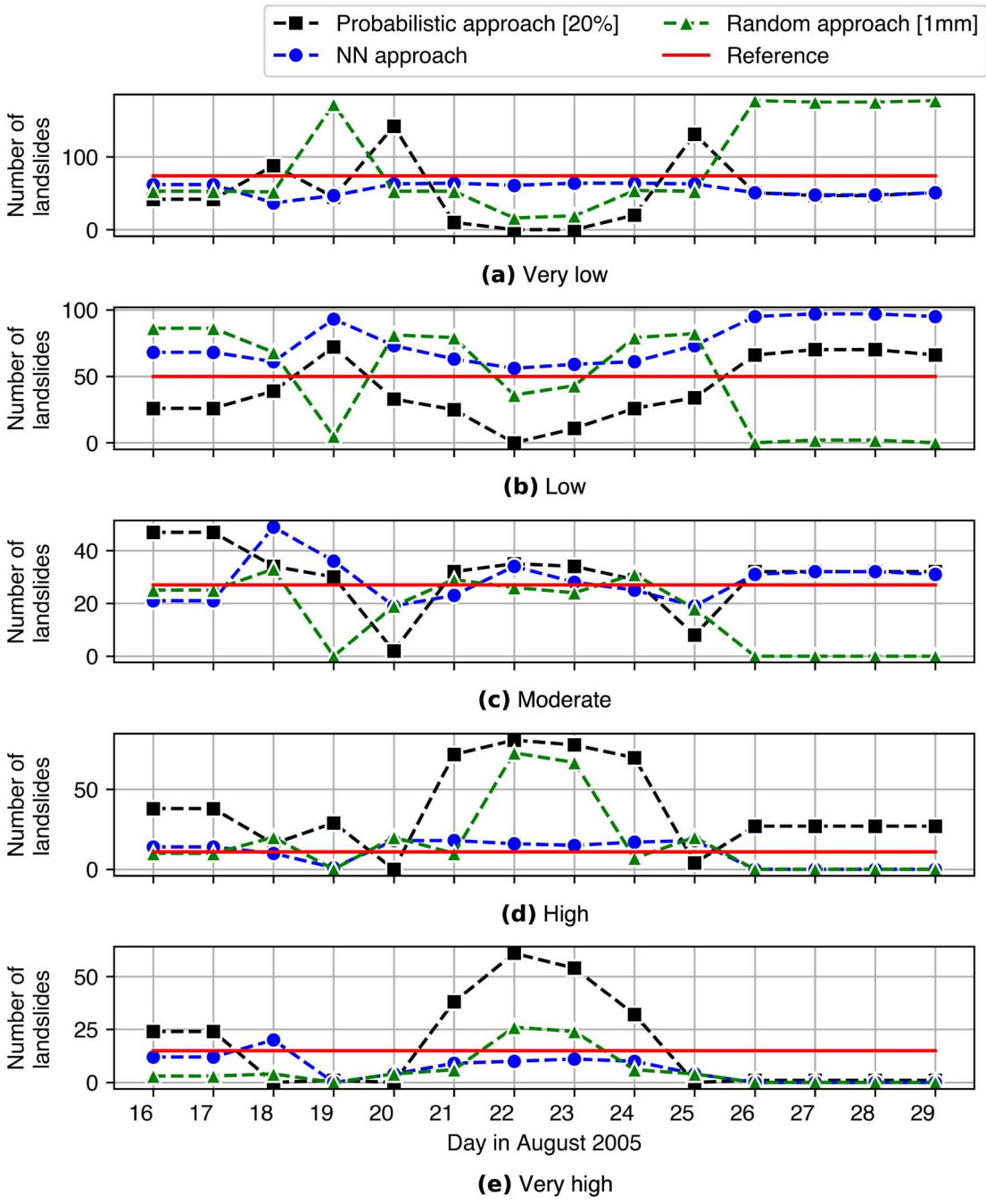

Figure 15. Comparison of the number of August 2005 landslides contained in the inventory of the canton Bern, that are assigned to the five different hazard classes for each approach. The red line marks the time-independent reference susceptibility map (see Section 3.1).

4. Discussion

The results of the presented test case provide many valuable insights into the advantages and disadvantages of the presented methodology. First of all, it can be concluded that ML has proven itself as a valuable tool for hazard prediction and early warning. Especially the broad range of precipitation values that triggered the landslides in the *Hangmuren* database (see Figure 5(a)) shows the difficulty of defining a specific precipitation threshold for a heterogeneous area. The support that ML could provide to early warning with a high spatial and temporal resolution has been demonstrated in this study.

The premise of this study is that the time-independent susceptibility assessment is often not sufficient due to the strong spatio-temporal characteristic of landslide occurrence. Figure 16 supports this claim with the low number of landslides in the Bern inventory that were triggered in areas of *high* or *very high* hazard according

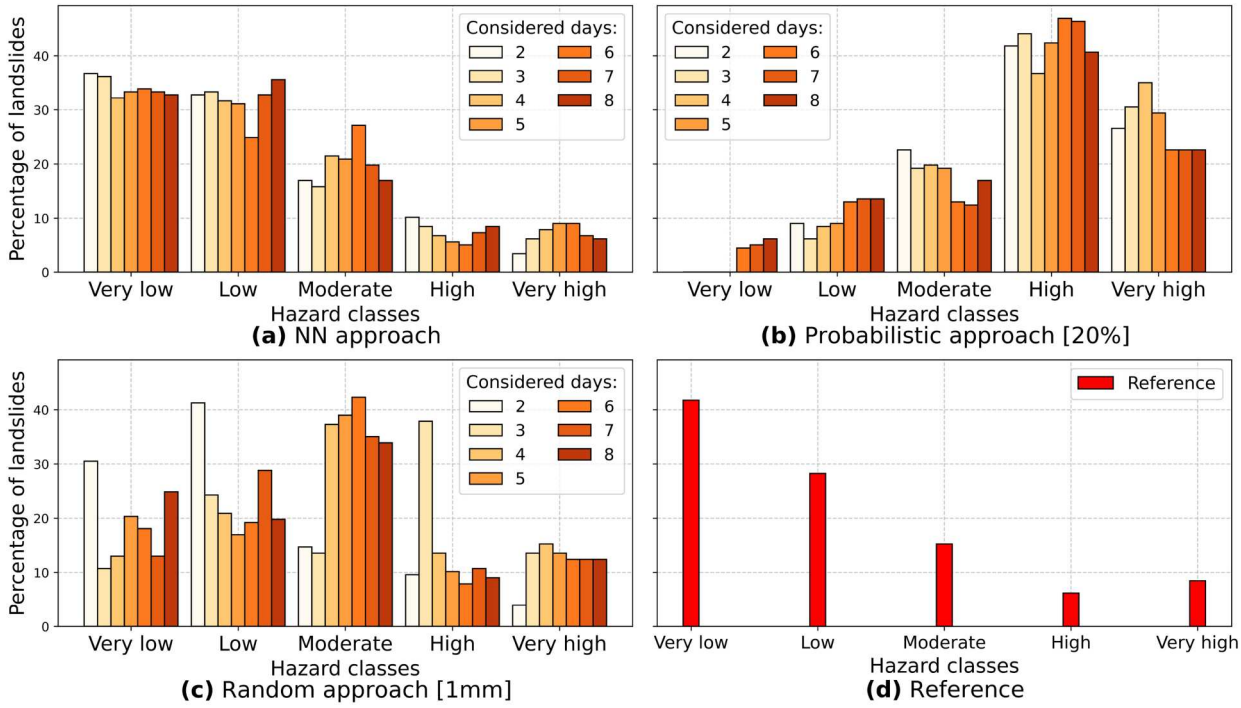

Figure 16. Comparison of the validation introduced in Section 3.3.1 using the landslide inventory of the canton Bern for different intervals of considered antecedent precipitation: (a) NN approach, (b) Probabilistic approach, (c) Random approach and (d) time-independent reference. For (a)–(c) time intervals of 2, 3, 4, 5, 6, 7 and 8 days are compared. For each approach to determine absence location precipitation the hazard map for 23 August 2005 was computed respecting each tested time interval of antecedent precipitation. From these maps the percentage of landslides in the inventory that fall into the different hazard classes are extracted.

to the time-independent reference. Our results, generally, underline the importance of the time-dependent precipitation in the modelling process with the in Figures 12–14 displayed spatio-temporal development of the hazard classification under changing precipitation conditions. To assess the suitability of the three approaches in more detail, next to the model quality determined through the conducted validation, the following characteristics of the generated hazard maps can be compared and discussed: (1) spatial variation of the hazard distribution under changing precipitation conditions, (2) temporal rate of these changes and (3) total size of the hazardous area. Due to the lack of studies for comparison, it is difficult to assess the reasonability of the temporal rate of the spatial changes over time. However, the changes in the spatial distribution themselves and the size of the area assigned to the different hazard classes can very well be discussed. We assume that a reasonable development is the increase of *moderate, high* and *very high* hazard areas during an intense rainfall event compared to before and after the event. Especially the behaviour of the results described in Section 3.2 for the Probabilistic approach (see Figure 11), but also the Random approach, fulfil this assumption. The NN approach responds the least to the changes in triggering conditions.

The reduced sensitivity of the NN approach is also reflected in the hindcast results, where the majority of landslides in the Bern inventory fall within lower hazard classes (see Figures 15 and 16). Additional evidence comes from the feature importance values generated through SHIRE. For the Random and Probabilistic approaches, precipitation is the most influential predictor (25.3 % and 27.5 %, respectively). In contrast, the NN approach assigns the parameter precipitation only 10.4 %, making it the fourth most important feature. This reduced importance indicates that the NN model relies less on precipitation than the other approaches, which explains its lower sensitivity to changes in rainfall conditions. Varying behaviour of the NN approach compared to the other approaches is already visible in the precipitation values determined for the absence locations (Figure 5).

They are higher and overall more wide-spread than the values determined based on the other two approaches, most likely due to the NN assigning very low precipitation probability thresholds (<5 %) for a substantial number of absence locations. This effect likely arises from the clustered nature of the landslide inventory that the NN is trained on. Many landslides contained occurred during extreme rainfall events and the exceedance probabilities associated with presence locations are consequently heavily skewed toward very

low values. During training, the NN therefore predominantly observes extreme-event patterns and learns that landslide-related rainfall is typically located in the tail of the distribution. When the NN is applied to absence locations with similar environmental characteristics, it frequently assigns very low predicted thresholds. Such low thresholds correspond to the highest quantiles of each absence location's precipitation distribution. As a result, the extraction step selects precipitation values that are substantially higher and more widely scattered than those produced by the other two approaches. This mechanism explains why the NN-derived precipitation ranges exceed those obtained via the Probabilistic and Random methods. Therefore, the observed behaviour is a result of how the NN amplifies the extreme precipitation patterns inherent in the clustered landslide data. The other approaches cannot amplify these extremes in the same way: the Probabilistic approach uses a fixed global threshold (here 20 %), and the Random approach samples directly from the empirical distribution. The NN, however, learns from the extreme-event signature and generalises it more broadly across the absence locations. Overall, although the NN approach does yield insufficient spatio-temporal hazard prediction for the present dataset, its inclusion in this study remains nevertheless valuable. With more spatially independent training data, the method has the potential to provide improved results and to further reduce subjectivity in the handling of absence locations for ML-based landslide hazard prediction.

Compared to the Random and especially the Probabilistic approach the time-independent assessment produces acceptable predictions before and after the intense rainfall event. However, it has the tendency to overestimate the size of the area of higher hazard classes and to underestimate the size of the lower class areas. The time-independent reference significantly underestimates *very high*, *high* and *moderate* hazard during the intense rainfall event. With regard to an EWS, this could lead to significant negative impact and highlights the advantages of spatio-temporal modelling. The Probabilistic approach, thereby, shows stronger sensitivity to precipitation changes. Compared to the Random approach, however, also more areas of higher hazard are predicted for the period after the intense rainfall event where only little rain occurred. We argue that, although it is reasonable for mostly lower hazard areas to be predicted in a drier context, the higher hazard classes present in the Probabilistic approach prediction is not a sign of insufficient model quality. The critical time during the intense rainfall event is most important and with regard to potential future application of ML for EWSs a conservative prediction might even be suitable.

Addressing the research gap we formulated in the beginning, namely how to enrich training data for ML-based landslide hazard prediction with spatio-temporal precipitation information, we, therefore, recommend applying the Probabilistic approach as it yielded strong validation results and the produced maps align with both domain knowledge and our expectations on the spatio-temporal variations of hazard classification. We attribute these qualities to the in the approach inherently included information on the precipitation history of the individual locations involved in model training. Nevertheless, also the Random approach shows very promising results. However, the results indicate that sampling from the adapted precipitation time series of this approach might not lead to the same degree of representativeness of the precipitation patterns as the Probabilistic approach. Independent of the choice of applied approach, we want to emphasise the importance of fine-tuning and careful choice of the applied precipitation or probability threshold. We assume the thresholds to be study-dependent, due to the influence of the distribution and location of the underlying landslide locations and suggest performing tests on suitable thresholds such as done in this study. This limits the generalizability of any fixed threshold and should be considered when extending the method to larger spatial domains. In particular, applying a uniform threshold, as done in the Probabilistic approach, is unlikely to remain appropriate if the spatial extent becomes too large or heterogeneous. In such cases, more adaptive approaches that allow thresholds to vary across space may be preferable. Although the NN approach displayed reduced sensitivity in the present study, its data-driven threshold assignment has the potential to better accommodate spatial heterogeneity in larger or more diverse regions. This highlights the importance of selecting strategies to define thresholds that reflect both the scale and the spatial complexity of the application.

5. Conclusion

This study demonstrates that ML can be a valuable tool for landslide hazard prediction. We presented and tested three approaches to sample precipitation values for Random Forest training data that are especially applicable for studies using a limited number of absence locations due to the reduced randomness during sampling. In this study, the Probabilistic approach, closely followed by the adapted Random approach, provide very promising results in the sense of the resulting hazard predictions fulfilling the domain knowledge as well as the required positive outcome of our validation strategy. Specifically, we observe that during the investigated intense rainfall

event, the size of the areas classified with *moderate, high* and *very high* hazard increased for the Probabilistic and Random approach. The NN approach, however, showed a reduced sensitivity to the changes in precipitation condition resulting in less significant changes related to the size of the differently classified areas. Our results also show how the different approaches influence the predicted hazard distribution before and after the intense rainfall event where low or no precipitation has been recorded. The Probabilistic approach predicts more areas of higher hazard for the period after the intense rainfall event compared to the Random approach. We underline the importance of adapting the strategies to the prevalent conditions of the AOI and the available data.

We acknowledge the limitations of our study especially regarding the possible lack of spatial representativeness of landslide locations. Nevertheless, our results show the potential of ML-based landslide hazard prediction also with regard to future applications in the context of EWSs. However, further research is needed to develop ML as a valid tool for this purpose:

- Refinement of the ML-based hazard prediction pipeline, e.g. in the area of strategic validation, for which advanced data products and landslide inventories are necessary. This strengthens trust and reliability of the system.
- Investigation of the integration of long-term climatological information to distinguish between dry and wet periods, enabling models to account for varying prevalent subsurface conditions that influence landslide initiation during triggering precipitation events. This would require landslide inventories covering events triggered under different climatological conditions.
- Incorporation of more physically-based hydrological variables, such as soil moisture, to better represent post-precipitation subsurface response processes that may improve model sensitivity and overall predictive performance. This would require large-scale subsurface information with appropriate spatio-temporal resolution.

Acknowledgments

This study was performed as part of the Helmholtz School for Data Science in Life, Earth and Energy (HDS-LEE).

Author contributions

CRediT: **AE:** Formal analysis, Investigation, Methodology, Software, Writing – original draft; **AY:** Conceptualization, Methodology, Supervision, Writing – review & editing; **RR:** Supervision, Writing – review & editing; **JK:** Funding acquisition, Resources, Supervision, Writing – review & editing

Disclosure statement

The authors report there are no competing interests to declare.

Funding

Funding has been provided through the German Federal Ministry for the Environment, Climate Action, Nature Conservation and Nuclear Safety under Grant No. 67KI2043 (KISTE project). Open access funding provided by the Open Access Publishing Fund of RWTH Aachen University.

Data availability statement

All data used in this study are publicly available and can be accessed using the sources and references provided in the manuscript.

ORCID

Ann-Kathrin Edrich http://orcid.org/0009-0003-3982-9318
Anil Yildiz http://orcid.org/0000-0002-2257-7025
Ribana Roscher http://orcid.org/0000-0003-0094-6210
Julia Kowalski http://orcid.org/0000-0003-4123-5896

References

Abraham, Minu Treesa, Manjunath Vaddapally, Neelima Satyam, and Biswajeet Pradhan. 2023. "Spatio-Temporal Landslide Forecasting Using Process-Based and Data-Driven Approaches: A Case Study from Western Ghats, India." *Catena* 223:106948. https://doi.org/10.1016/j.catena.2023.106948.

Aleotti, Pietro. 2004. "A Warning System for Rainfall-Induced Shallow Failures." *Engineering Geology*73 (3-4): 247–265. https://doi.org/10.1016/j.enggeo.2004.01.007.

Ballabio, Cristiano, Panos Panagos, and Luca Monatanarella. 2016. "Mapping Topsoil Physical Properties at European Scale Using the LUCAS Database." *Geoderma* 261:110–123. https://doi.org/10.1016/j.geoderma.2015.07.006.

Beniston, Martin. 2006. "August 2005 Intense Rainfall Event in Switzerland: Not Necessarily an Analog for Strong Convective Events in a Greenhouse Climate." *Geophysical Research Letters* 33 (5). https://doi.org/10.1029/2005GL025573.

Biswas, Nishan Kumar, Thomas A. Stanley, Dalia B. Kirschbaum, Pukar M. Amatya, Chinaporn Meechaiya, Ate Poortinga, and Peeranan Towashiraporn. 2022. "A Dynamic Landslide Hazard Monitoring Framework for the Lower Mekong Region." *Frontiers in Earth Science* 10:1057796. https://doi.org/10.3389/feart.2022.1057796.

Bogaard, Thom, and Roberto Greco. 2018. "Invited Perspectives: Hydrological Perspectives on Precipitation Intensity-Duration Thresholds for Landslide Initiation: Proposing Hydro-Meteorological Thresholds." *Natural*

*Hazards and Earth System Sciences*18 (1): 31–39. https://doi.org/10.5194/nhess-18-31-2018.

Caine, Nel. 1980. "The Rainfall Intensity-Duration Control of Shallow Landslides and Debris Flows." *Geografiska Annaler: Series A, Physical Geography* 62 (1-2): 23–27. https://doi.org/10.1080/04353676.1980.11879996.

Casagli, Nicola, Emanuele Intrieri, Tommaso Carlà, Federico Di Traglia, William Frodella, Giovanni Gigli, Luca Lombardi, Massimiliano Nocentini, Federico Raspini, and Veronica Tofani. 2021. "Monitoring and Early Warning Systems: Applications and Perspectives." In *Understanding and Reducing Landslide Disaster Risk*, edited by Nicola Casagli, Veronica Tofani, Kyoji Sassa, Peter T. Bobrowsky, and Kaoru Takara, Vol. 3, 1–21. Cham: Springer International Publishing.

Chikalamo, Elias E., Olga C. Mavrouli, Janneke Ettema, Cees J. van Westen, Agus S. Muntohar, and Akhyar Mustofa. 2020. "Satellite-Derived Rainfall Thresholds for Landslide Early Warning in Bogowonto Catchment, Central Java, Indonesia." *International Journal of Applied Earth Observation and Geoinformation* 89:102093. https://doi.org/10.1016/j.jag.2020.102093.

Conforti, Massimo, Stefania Pascale, Gaetano Robustelli, and Francesco Sdao. 2014. "Evaluation of Prediction Capability of the Artificial Neural Networks for Mapping Landslide Susceptibility in the Turbolo River Catchment (northern Calabria, Italy)." *Catena*113:236–250. https://doi.org/10.1016/j.catena.2013.08.006.

Copernicus Land Monitoring Service. 2018. "High Resolution Layer: Tree Cover Density (TCD) 2018" (dataset). Accessed September, 2021. https://land.copernicus.eu/pan-european/high-resolution-layers/forests/tree-cover-density/status-maps/tree-cover-density-2018?tab=metadata.

Dahal, Ashok, Hakan Tanyas, Cees van Westen, Mark van der Meijde, Paul Martin Mai, Raphaël Huser, and Luigi Lombardo. 2024. "Space–time Landslide Hazard Modeling via Ensemble Neural Networks." *Natural Hazards and Earth System Sciences* 24 (3): 823–845. https://doi.org/10.5194/nhess-24-823-2024.

Dai, F. C., and C. F. Lee. 2003. "A Spatiotemporal Probabilistic Modelling of Storm-Induced Shallow Landsliding Using Aerial Photographs and Logistic Regression." *Earth Surface Processes and Landforms: The Journal of the British Geomorphological Research Group* 28 (5): 527–545. https://doi.org/10.1002/esp.456.

Dang, Viet-Hung, Tien Bui Dieu, Xuan-Linh Tran, and Nhat-Duc Hoang. 2019. "Enhancing the Accuracy of Rainfall-Induced Landslide Prediction along Mountain Roads with a GIS-based Random Forest Classifier." *Bulletin of Engineering Geology and the Environment* 78 (4): 2835–2849. https://doi.org/10.1007/s10064-018-1273-y.

Dilley, Maxx, Robert S. Chen, Uwe Deichmann, Arthur L. Lerner-Lam, and Margaret Arnold. 2005. "Natural Disaster Hotspots: A Global Risk Analysis." Technical Report. Washington, DC: The World Bank. http://hdl.handle.net/10986/7376.

Edrich, Ann-Kathrin, Anil Yildiz, and Julia Kowalski. 2023. "Landslide Susceptibility and Hazard Mapping Framework." Access under https://doi.org/10.6084/m9.figshare.24339643.

Edrich, Ann-Kathrin, Anil Yildiz, Ribana Roscher, Alexander Bast, Frank Graf, and Julia Kowalski. 2024. "A Modular Framework for FAIR Shallow Landslide Susceptibility Mapping Based on Machine Learning." *Natural Hazards* 120 (9): 8953–8982. https://doi.org/10.1007/s11069-024-06563-8.

Emberson, Robert, Dalia Kirschbaum, and Thomas Stanley. 2020. "New Global Characterisation of Landslide Exposure." *Natural Hazards and Earth System Sciences* 20 (12): 3413–3424. https://doi.org/10.5194/nhess-20-3413-2020.

Emberson, Robert, Dalia Kirschbaum, and Thomas Stanley. 2021. "Global Connections between El Nino and Landslide Impacts." *Nature Communications* 12 (1): 2262. https://doi.org/10.1038/s41467-021-22398-4.

Federal Office of Topography swisstopo. 2005. "DHM25" (dataset). Accessed September, 2021. https://www.swisstopo.admin.ch/en/geodata/height/dhm25.html.

Federal Office of Topography Swisstopo. 2021. "swissBOUNDARIES3D: Administrative Units of Switzerland and Liechtenstein" (dataset). Accessed April, 2021. https://www.swisstopo.admin.ch/en/landscape-model-swissboundaries3d.

Fell, Robin, Jordi Corominas, Christophe Bonnard, Leonardo Cascini, Eric Leroi, and William Z. Savage. 2008. "Guidelines for Landslide Susceptibility, Hazard and Risk Zoning for Land Use Planning." *Engineering Geology* 102 (3-4): 85–98. https://doi.org/10.1016/j.enggeo.2008.03.022.

Frattini, Paolo, Giovanni Crosta, and Rosanna Sosio. 2009. "Approaches for Defining Thresholds and Return Periods for Rainfall-Triggered Shallow Landslides." *Hydrological Processes: An International Journal* 23 (10): 1444–1460. https://doi.org/10.1002/hyp.7269.

Guo, Zizheng, Mengchen Cheng, Yunge Wang, Gang Xu, Yuhua Zhang, and Chong Xu. 2025. "Landslide Hazard Prediction under an Extreme Rainfall Scenario by considering Multiple Timescale Rainfalls and Effective Recharge." *Georisk: Assessment and Management of Risk for Engineered Systems and Geohazards* 19 (4): 775–803. https://doi.org/10.1080/17499518.2025.2570863.

Guzzetti, Fausto, Stefano Luigi Gariano, Silvia Peruccacci, Maria Teresa Brunetti, Ivan Marchesini, Mauro Rossi, and Massimo Melillo. 2020. "Geographical Landslide Early Warning Systems." *Earth-Science Reviews* 200:102973. https://doi.org/10.1016/j.earscirev.2019.102973.

Guzzetti, Fausto, Silvia Peruccacci, Mauro Rossi, and Colin P. Stark. 2007. "Rainfall Thresholds for the Initiation of Landslides in Central and Southern Europe." *Meteorology and Atmospheric Physics* 98 (3-4): 239–267. https://doi.org/10.1007/s00703-007-0262-7.

Hählen, Nils. 2023. "Kennzahlen Zu Spontanen Rutschungen Im Kanton Bern Mit Schwerpunkt Auf Alpen Und Voralpen." Source Provides Poster, Report and Data. Accessed Marh 31, 2025. https://www.researchgate.net/publication/368510037_Kennzahlen_zu_spontanen_Rutschungen_im_Kanton_Bern_mit_Schwerpunkt_auf_Alpen_und_Voralpen.

Harilal, Geethu Thottungal, Dhanya Madhu, Maneesha Vinodini Ramesh, and Divya Pullarkatt. 2019. "Towards Establishing Rainfall Thresholds for a Real-Time Landslide Early Warning System in Sikkim, India." *Landslides* 16 (12): 2395–2408. https://doi.org/10.1007/s10346-019-01244-1.

Hemalatha, T., Maneesha Vinodini Ramesh, and Venkat P. Rangan. 2019. "Effective and Accelerated Forewarning of Landslides Using Wireless Sensor Networks and Machine

Learning." *IEEE Sensors Journal* 19 (21): 9964–9975. https://doi.org/10.1109/JSEN.2019.2928358.

Hilker, Nadine, Christoph Hegg, and Massimiliano Zappa. 2008. "Unwetterschäden in Der Schweiz 1972-2007. Mit Besonderer Betrachtung Des August-Hochwassers 2005." In *Interpraevent 2008 – Conference Proceedings*, Vol. 1, 99–110. Accessed May 10, 2024. https://archive.interpraevent.at/palm-cms/upload_files/Publikationen/Tagungsbeitraege/2008_1_99.pdf.

Hong, Haoyuan, Yamin Miao, Junzhi Liu, and A.-Xing Zhu. 2019. "Exploring the Effects of the Design and Quantity of Absence Data on the Performance of Random Forest-Based Landslide Susceptibility Mapping." *Catena* 176:45–64. https://doi.org/10.1016/j.catena.2018.12.035.

Ishibashi, Hiroki. 2023. "Framework for Risk Assessment of Economic Loss from Structures Damaged by Rainfall-Induced Landslides Using Machine Learning." *Georisk: Assessment and Management of Risk for Engineered Systems and Geohazards* 18 (1): 228–243. https://doi.org/10.1080/17499518.2023.2288606.

Jones, Joshua Nathan, Sarah Jean Boulton, Georgina L. Bennett, Martin Stokes, and Michael R. Z. Whitworth. 2021. "Temporal Variations in Landslide Distributions following Extreme Events: Implications for Landslide Susceptibility Modeling." *Journal of Geophysical Research: Earth Surface*126 (7): e2021JF006067. https://doi.org/10.1029/2021JF006067.

Jordanova, Galena, Stefano Luigi Gariano, Massimo Melillo, Silvia Peruccacci, Maria Teresa Brunetti, and Mateja Jemec Auflič. 2020. "Determination of Empirical Rainfall Thresholds for Shallow Landslides in Slovenia Using an Automatic Tool." *Water* 12 (5): 1449. https://doi.org/10.3390/w12051449.

Kashyap, Rahul, Arvind Chandra Pandey, and Bikash Ranjan Parida. 2021. "Spatio-Temporal Variability of Monsoon Precipitation and Their Effect on Precipitation Triggered Landslides in Relation to Relief in Himalayas." *Spatial Information Research* 29 (6): 857–869. https://doi.org/10.1007/s41324-021-00392-8.

Lagomarsino, Daniela, Samuele Segoni, Riccardo Fanti, and Filippo Catani. 2013. "Updating and Tuning a Regional-Scale Landslide Early Warning System." *Landslides* 10 (1): 91–97. https://doi.org/10.1007/s10346-012-0376-y.

Lateltin, Olivier, Christoph Haemmig, Hugo Raetzo, and Christophe Bonnard. 2005. "Landslide Risk Management in Switzerland." *Landslides* 2 (4): 313–320. https://doi.org/10.1007/s10346-005-0018-8.

Lee, Jung-Hyun, Hanbeen Kim, Hyuck-Jin Park, and Jun-Haeng Heo. 2021. "Temporal Prediction Modeling for Rainfall-Induced Shallow Landslide Hazards Using Extreme Value Distribution." *Landslides* 18 (1): 321–338. https://doi.org/10.1007/s10346-020-01502-7.

Li, Bohao, Kai Liu, Ming Wang, Qian He, Ziyu Jiang, Weihua Zhu, and Ningning Qiao. 2022. "Global Dynamic Rainfall-Induced Landslide Susceptibility Mapping Using Machine Learning." *Remote Sensing*14 (22): 5795. https://doi.org/10.3390/rs14225795.

Liu, Qiang, Aiping Tang, and Delong Huang. 2023. "Exploring the Uncertainty of Landslide Susceptibility Assessment Caused by the Number of Non–landslides." *Catena* 227:107109. https://doi.org/10.1016/j.catena.2023.107109.

Liu, Yanhui, Junbao Huang, Ruihua Xiao, Shiwei Ma, and Pinggen Zhou. 2022. "Research on a Regional Landslide Early-Warning Model Based on Machine Learning – A Case Study of Fujian Province, China." *Forests* 13 (12): 2182. https://doi.org/10.3390/f13122182.

Ma, Tuhua, Changjiang Li, Zhiming Lu, and Baoxin Wang. 2014. "An Effective Antecedent Precipitation Model Derived from the Power-Law Relationship between Landslide Occurrence and Rainfall Level." *Geomorphology* 216:187–192. https://doi.org/10.1016/j.geomorph.2014.03.033.

Mastrantoni, G., G. M. Marmoni, C. Esposito, F. Bozzano, G. Scarascia Mugnozza, and P. Mazzanti. 2023. "Reliability Assessment of Open-Source Multiscale Landslide Susceptibility Maps and Effects of Their Fusion." *Georisk: Assessment and Management of Risk for Engineered Systems and Geohazards*18 (3): 628–645. https://doi.org/10.1080/17499518.2023.2251139.

McColl, Samuel T. 2015. "Landslide Causes and Triggers." In *Landslide Hazards, Risks, and Disasters*, edited by John F. Shroder and Tim Davies, Hazards and Disasters Series, 17–42. Boston: Academic Press.

Melillo, Massimo, Maria Teresa Brunetti, Silvia Peruccacci, Stefano Luigi Gariano, and Fausto Guzzetti. 2015. "An Algorithm for the Objective Reconstruction of Rainfall Events Responsible for Landslides." *Landslides* 12 (2): 311–320. https://doi.org/10.1007/s10346-014-0471-3.

Miyagi, Toyohiko. 2021. "Landslide Recognition and Mapping for Slope Disaster Risk Reduction and Management–Keynote Speech." In *Understanding and Reducing Landslide Disaster Risk: From Mapping to Hazard and Risk Zonation*, edited by Fausto Guzzetti, Snježana Mihalić Arbanas, Paola Reichenbach, Kyoji Sassa, Peter T. Bobrowsky, and Kaoru Takara, Vol. 2, 9–31. Cham: Springer International Publishing.

Mondini, Alessandro C., Fausto Guzzetti, and Massimo Melillo. 2023. "Deep Learning Forecast of Rainfall-Induced Shallow Landslides." *Nature Communications* 14 (1): 2466. https://doi.org/10.1038/s41467-023-38135-y.

Montrasio, Lorella, and Roberto Valentino. 2008. "A Model for Triggering Mechanisms of Shallow Landslides." *Natural Hazards and Earth System Sciences* 8 (5): 1149–1159. https://doi.org/10.5194/nhess-8-1149-2008.

Moon, Seung-Hyun, Yong-Hyuk Kim, Yong Hee Lee, and Byung-Ro Moon. 2019. "Application of Machine Learning to an Early Warning System for Very short-term Heavy Rainfall." *Journal of Hydrology*568:1042–1054. https://doi.org/10.1016/j.jhydrol.2018.11.060.

Moreno, Adam, and Hubert Hasenauer. 2016. "Spatial Downscaling of European Climate Data." *International Journal of Climatology* 36 (3): 1444–1458. https://doi.org/10.1002/joc.4436.

Ng, Charles Wang Wai, Bin Yang, Z. Q. Liu, J. S. H. Kwan, and Lei Chen. 2021. "Spatiotemporal Modelling of Rainfall-Induced Landslides Using Machine Learning." *Landslides* 18 (7): 2499–2514. https://doi.org/10.1007/s10346-021-01662-0.

Nocentini, Nicola, Ascanio Rosi, Samuele Segoni, and Riccardo Fanti. 2023. "Towards Landslide Space-Time Forecasting through Machine Learning: The Influence of Rainfall Parameters and Model Setting." *Frontiers in Earth Science* 11:1152130. https://doi.org/10.3389/feart.2023.1152130.

Oguz, Emir Ahmet, Rasmus E. Benestad, Kajsa M. Parding, Ivan Depina, and Vikas Thakur. 2024. "Quantification of Climate Change Impact on Rainfall-Induced Shallow Landslide Susceptibility: A Case Study in Central Norway." *Georisk: Assessment and Management of Risk for Engineered Systems and Geohazards* 18 (2): 467–490. https://doi.org/10.1080/17499518.2023.2283848.

Palladino, Michael Rosa, A. Viero, L. Turconi, M. T. Brunetti, S. Peruccacci, M. Melillo, F. Luino, A. M. Deganutti, and F. Guzzetti. 2018. "Rainfall Thresholds for the Activation of Shallow Landslides in the Italian Alps: The Role of Environmental Conditioning Factors." *Geomorphology* 303:53–67. https://doi.org/10.1016/j.geomorph.2017.11.009.

Panagos, Panos, Pasquale Borrelli, Katrin Meusburger, Bofu Yu, Andreas Klik, Kyoung Jae Lim, Jae E. Yang. 2017. "Global Rainfall Erosivity Assessment Based on High-Temporal Resolution Rainfall Records." *Scientific Reports* 7 (1): 4175. https://doi.org/10.1038/s41598-017-04282-8.

Piciullo, Luca, Michele Calvello, and José Mauricio Cepeda. 2018. "Territorial Early Warning Systems for Rainfall-Induced Landslides." *Earth-Science Reviews* 179:228–247. https://doi.org/10.1016/j.earscirev.2018.02.013.

Pucher, C. 2023. "Description and Evaluation of Downscaled Daily Climate Data Version 4" (dataset). Accessed November, 2023. https://doi.org/10.6084/m9.figshare.22962671.v1.

QGIS Development Team. 2020. "QGIS Geographic Information System." Accessed December, 2023 https://qgis.org/.

Reichenbach, Paola, Mauro Rossi, Bruce D. Malamud, Monika Mihir, and Fausto Guzzetti. 2018. "A Review of Statistically-Based Landslide Susceptibility Models." *Earth-Science Reviews* 180:60–91. https://doi.org/10.1016/j.earscirev.2018.03.001.

Ren, Tianhe, Liang Gao, and Wenping Gong. 2024. "An Ensemble of Dynamic Rainfall Index and Machine Learning Method for Spatiotemporal Landslide Susceptibility Modeling." *Landslides* 21 (2): 257–273. https://doi.org/10.1007/s10346-023-02152-1.

Rickli, Christian, Frank Graf, Peter Bebi, Alexander Bast, Bernard Loup, and Brian McArdell. 2019. "Schützt Der Wald Vor Rutschungen? Hinweise Aus Der WSL-Rutschungsdatenbank." *Schweizerische Zeitschrift Für Forstwesen* 170 (6): 310–317. https://doi.org/10.3188/szf.2019.0310.

Segoni, Samuele, Alessandro Battistini, Guglielmo Rossi, Ascanio Rosi, Daniela Lagomarsino, Filippo Catani, Sandro Moretti, and Nicola Casagli. 2015. "An Operational Landslide Early Warning System at Regional Scale Based on Space–time-Variable Rainfall Thresholds." *Natural Hazards and Earth System Sciences* 15 (4): 853–861. https://doi.org/10.5194/nhess-15-853-2015.

Segoni, Samuele, Luca Piciullo, and Stefano Luigi Gariano. 2018. "A Review of the Recent Literature on Rainfall Thresholds for Landslide Occurrence." *Landslides* 15 (8): 1483–1501. https://doi.org/10.1007/s10346-018-0966-4.

Sidle, Roy C., and Hirotaka Ochiai. 2006. *Landslides : Processes, Prediction, and Land Use*. Water Resources Monograph. Washington, DC: American Geophysical Union.

Stanley, Thomas A., Dalia B. Kirschbaum, Garrett Benz, Robert A. Emberson, Pukar M. Amatya, William Medwedeff, and Marin K. Clark. 2021. "Data-Driven Landslide Nowcasting at the Global Scale." *Frontiers in Earth Science* 9: 640043. https://doi.org/10.3389/feart.2021.640043.

Steger, Stefan, Mateo Moreno, Alice Crespi, Stefano Luigi Gariano, Maria Teresa Brunetti, Massimo Melillo, Silvia Peruccacci. 2024. "Adopting the Margin of Stability for Space–time Landslide Prediction–A Data-Driven Approach for Generating Spatial Dynamic Thresholds." *Geoscience Frontiers* 15 (5):101822. https://doi.org/10.1016/j.gsf.2024.101822.

Sudani, Prashant, K. A. Patil, and Y. A. Kolekar. 2021. "Historical Development of Landslide Early Warning System (LEWS): A Review." In *Indian Geotechnical Conference*, 263–277. Springer.

Sun, Deliang, Qingyu Gu, Haijia Wen, Shuxian Shi, Changlin Mi, and Fengtai Zhang. 2022. "A Hybrid Landslide Warning Model Coupling Susceptibility Zoning and Precipitation." *Forests* 13 (6): 827. https://doi.org/10.3390/f13060827.

Swiss Federal Institute for Forest, Snow and Landscape Research WSL, Mountain Hydrology and Mass Movements. 2023. "Datenquelle Hangmuren-Datenbank" (dataset). Accessed March 8, 2021. https://hangmuren.wsl.ch/.

Tehrani, Faraz S., Michele Calvello, Zhongqiang Liu, Limin Zhang, and Suzanne Lacasse. 2022. "Machine Learning and Landslide Studies: Recent Advances and Applications." *Natural Hazards* 114 (2): 1197–1245. https://doi.org/10.1007/s11069-022-05423-7.

Terlien, Mark T. J. 1998. "The Determination of Statistical and Deterministic Hydrological Landslide-Triggering Thresholds." *Environmental Geology*35 (2-3): 124–130. https://doi.org/10.1007/s002540050299.

Thiebes, B., and T. Glade. 2018. "Landslide Early Warning Systems – Fundamental Concepts and Innovative Applications." In *Landslides and Engineered Slopes. Experience, Theory and Practice*, 1903–1911. CRC Press.

Thirugnanam, Hemalatha, Maneesha Vinodini Ramesh, and Venkat P. Rangan. 2020. "Enhancing the Reliability of Landslide Early Warning Systems by Machine Learning." *Landslides* 17 (9): 2231–2246. https://doi.org/10.1007/s10346-020-01453-z.

Tiranti, Davide, and Davide Rabuffetti. 2010. "Estimation of Rainfall Thresholds Triggering Shallow Landslides for an Operational Warning System Implementation." *Landslides* 7 (4): 471–481. https://doi.org/10.1007/s10346-010-0198-8.

Tonini, Marj, and Mariaelena Cama. 2019. "Spatio-Temporal Pattern Distribution of Landslides Causing Damage in Switzerland." *Landslides* 16 (11): 2103–2113. https://doi.org/10.1007/s10346-019-01236-1.

Tóth, Brigitta, Melanie Weynants, László Pásztor, and Tomislav Hengl. 2017. "3D Soil Hydraulic Database of Europe at 250 M Resolution." *Hydrological Processes* 31 (14): 2662–2666. https://doi.org/10.1002/hyp.11203.

Turner, Alan Keith. 2018. "Social and Environmental Impacts of Landslides." *Innovative Infrastructure Solutions* 3 (1): 1–25. https://doi.org/10.1007/s41062-018-0175-y.

Uwihirwe, Judith, Markus Hrachowitz, and Thom A. Bogaard. 2020. "Landslide Precipitation Thresholds in Rwanda." *Landslides* 17 (10): 2469–2481. https://doi.org/10.1007/s10346-020-01457-9.

Van Genuchten, M. T. 1980. "A Closed-Form Equation for Predicting the Hydraulic Conductivity of Unsaturated Soils." *Soil Science Society of America Journal* 44 (5): 892–898. https://doi.org/10.2136/sssaj1980.03615995004400050002x.

van Natijne, Adriaan L., Roderik C. Lindenbergh, and Thom A. Bogaard. 2020. "Machine Learning: New Potential for Local and Regional Deep-Seated Landslide Nowcasting." *Sensors* 20 (5): 1425. https://doi.org/10.3390/s20051425.

Van Westen, Cees J., Enrique Castellanos, and Sekhar L. Kuriakose. 2008. "Spatial Data for Landslide Susceptibility, Hazard, and Vulnerability Assessment: An Overview." *Engineering Geology* 102 (3-4): 112–131. https://doi.org/10.1016/j.enggeo.2008.03.010.

Vasu, Nikhil Nedumpallile, Seung-Rae Lee, Ananta Man Singh Pradhan, Yun-Tae Kim, Sin-Hang Kang, and Deuk-Hwan Lee. 2016. "A New Approach to Temporal Modelling for Landslide Hazard Assessment Using an Extreme Rainfall Induced-Landslide Index." *Engineering Geology* 215:36–49. https://doi.org/10.1016/j.enggeo.2016.10.006.

Vilímek, Vit, Josef Hanzlík, Ivan Sládek, Milada Šandov, and Nelson Santillán. 2013. "The Share of Landslides in the Occurrence of Natural Hazards and the Significance of El Niño in the Cordillera Blanca and Cordillera Negra Mountains, Peru." In *Landslides: Global Risk Preparedness*, edited by Kyoji Sassa, Badaoui Rouhban, Sálvano Briceño, Mauri McSaveney, and Bin He, 133–148. https://doi.org/10.1007/978-3-642-22087-6_9.

Vishnu, C. L., T. Oommen, Snehamoy Chatterjee, and K. S. Sajinkumar. 2022. "Challenges of Modeling Rainfall Triggered Landslides in a Data-Sparse Region: A Case Study from the Western Ghats, India." *Geosystems and Geoenvironment* 1 (3):100060. https://doi.org/10.1016/j.geogeo.2022.100060.

Wang, Haojie, Limin Zhang, Hongyu Luo, Jian He, and Raymond Wai Man Cheung. 2021. "AI-powered Landslide Susceptibility Assessment in Hong Kong." *Engineering Geology* 288:106103. https://doi.org/10.1016/j.enggeo.2021.106103.

Xiao, Te, Li Min Zhang, Raymond Wai Man Cheung, and Suzanne Lacasse. 2022. "Predicting Spatio-Temporal Man-Made Slope Failures Induced by Rainfall in Hong Kong Using Machine Learning Techniques." *Géotechnique* 73:749–765. https://doi.org/10.1680/jgeot.21.00160.

Xie, Chenchen, Chong Xu, Xiwei Xu, Yuandong Huang, Zhiqiang Zhang, Hao Li, Hourong Zhang, and Dengjie Zhu. 2025. "Comprehensive Analysis and Assessment of Extreme Rainfall-Induced Clustered Landslides: A Case Study of Southern Qingyuan City, Guangdong Province, China, in June 2020." *Georisk: Assessment and Management of Risk for Engineered Systems and Geohazards*1–23. https://doi.org/10.1080/17499518.2025.2563759.

Yuniawan, Ragil Andika, Ahmad Rifa'ı, Fikri Faris, Andy Subiyantoro, Ratna Satyaningsih, Alidina Nurul Hidayah, Rokhmat Hidayat. 2022. "Revised Rainfall Threshold in the Indonesian Landslide Early Warning System." *Geosciences* 12 (3): 129. https://doi.org/10.3390/geosciences12030129.

Zhang, Yang, Weicheng Wu, Yaozu Qin, Ziyu Lin, Guiliang Zhang, Renxiang Chen, Yong Song. 2020. "Mapping Landslide Hazard Risk Using Random Forest Algorithm in Guixi, Jiangxi, China." *ISPRS International Journal of Geo-Information* 9 (11): 695. https://doi.org/10.3390/ijgi9110695.

Zhu, A.-Xing, Yamin Miao, Junzhi Liu, Shibiao Bai, Canying Zeng, Tianwu Ma, and Haoyuan Hong. 2019. "A Similarity-Based Approach to Sampling Absence Data for Landslide Susceptibility Mapping Using Data-Driven Methods." *Catena* 183:104188. https://doi.org/10.1016/j.catena.2019.104188.

Zieher, Thomas, Frank Perzl, Monika Rössel, Martin Rutzinger, Gertraud Meißl, Gerhard Markart, and Clemens Geitner. 2016. "A Multi-annual Landslide Inventory for the Assessment of Shallow Landslide Susceptibility–Two Test Cases in Vorarlberg, Austria." *Geomorphology* 259:40–54. https://doi.org/10.1016/j.geomorph.2016.02.008.